Sudan University of Science and Technology

College of Graduate Studies

The Effect of Change of Particle Nano Size and Concentration of Fe_3O_4 and Ni_2O_3 on Optical and Magnetic Properties Using XRD, SEM and UV-VIS

تأثير تغيير الحجم النانوي و التركيز لاوكسيد الحديد و اوكسيد النيكل(Fe_3O_4 , Ni_2O_3) علي الخصائص الضوئية و المغنطيسية باستخدام تقنية حيود الاشعة السينية و المجهر الالكتروني الماسح وتقنية طيف الاشعة فوق البنفسجية

Thesis Submitted in Fulfillment of the Requirements for the Degree of Ph.D. in physics

By:

Emtithal Ahmed Jadallah Ahmed

Msc./ Bsc. in Physics

Supervisor:

Dr. Ahmed Elhassan Elfaki Idries

Co-Supervisor:

Prof. Mubarak Dirar Abd-Alla

May 2019

الآية

قال تعالى: ((لَقَدْ أَرْسَلْنَا رُسُلَنَا بِالْبَيِّنَاتِ وَأَنزَلْنَا مَعَهُمُ الْكِتَابَ وَالْمِيزَانَ لِيَقُومَ النَّاسُ بِالْقِسْطِ وَأَنزَلْنَا الْحَدِيدَ فِيهِ بَأْسٌ شَدِيدٌ وَمَنَافِعُ لِلنَّاسِ وَلِيَعْلَمَ اللَّهُ مَن يَنصُرُهُ وَرُسُلَهُ بِالْغَيْبِ إِنَّ اللَّهَ قَوِيٌّ عَزِيزٌ)) (25)

صدق الله العظيم

سورة الحديد

Dedication

I dedicate this thesis to my mother and father, my dear sisters and brothers to my dear husband and my lovely kids and every person who helped me to finish this work.

Acknowledgment

Firstly, I would like to thank Allah almighty for making this work possible. Secondly, I would like to express my gratitude to my supervisor's prof. Mubarak Dirar, Dr. Abdalsakhi Abdallah and Dr. Ahmed Elfaki for their supervision, valuable advice, kind treatment and guidance during my work and to all whom support me. Thanks extend also to Sudan University of Science and Technology, Graduate College, Faculty of Sciences, Physics department for encouragements and facilities.

Abstract

The aim of this work is to find the optical parameters like absorption coefficient and energy gap and to find the electric permittivity and magnetic permeability for (Fe_3O_4 and Ni_2O_3) Nanomaterial thin films that were deposited on ITO glass substrate, ten samples were prepared by sol-gel method with deferent concentrations (55.25, 78.7, 90.9 144.9 and 263.15) mg/cm^2 for each nanomaterial. The Nano crystal size of the deposited was found by the XRD technique. The UV-VIS spectrum was used to find absorption coefficient, energy gap refractive index and electric permittivity. The magnetic permeability was found by using the relation between refractive index and electric permittivity beside magnetic permeability. For Fe_3O_4 the electric permittivity and magnetic permeability were shown to increase when the concentration of Nano crystal decreases. However for Ni_2O_3 the electric permittivity and magnetic permeability increases upon increasing the molecular concentration. For all samples the absorption coefficient decreases upon increasing the concentration, while the energy gap increases with concentration. The Fe and Ni properties when they are mixed together is also needed. The results obtained can be applied for electric generation and magnetic resonance imaging.

المستخلص

الهدف من هذا البحث هو ايجاد الخصائص الضوئية مثل معامل الامتصاص و فجوة الطاقة وايضا ايجاد السماحية الكهربية و النفاذية المغنطيسية لاكاسيد النيكل والحديد النانوية التى رسبت على شرائح اول اكسيد الانديوم تيتانيوم في عشرة عينات، خمسة عينات لكل اكسيد بطريقة المحلول و الجلاتين بتراكيز مختلفة (55.25, 78.7, 90.9, 263.15) جم/سم^2 لكل مادة. وجد حجم البلورة النانوي باستخدام تقنية حيود الاشعة السينية. استخدمت تقنية طيف الاشعة فوق البنفسجية لايجاد معامل الامتصاص و فجوة الطاقة و معامل الانكسار و السماحية الكهربية. النفاذية المغنطيسية وجد باستخدام العلاقات بين هذه الخواص و معامل الانكسار. بالنسبة لاكسيد الحديد وجد ان السماحية الكهربية و النفاذية المغنطيسية تزيد بنقصان التركيز. اما بالنسبة لاكسيد النيكل وجد ان السماحية الكهربية و النفاذية المغنطيسية تزيد بزيادة التركيز. لكل العينات معامل الامتصاص ينقص بزيادة التركيز بينما فجوة الطاقة تزيد بزيادة التركيز. في بحوث قادمة يمكن دمج خصائص الحديد والنيكل. النتائج المتحصل عليها يمكن تطبيقها في المولدات الكهربية و التصوير بالرنين المغنطيسي.

Table of Contents

List of Tables

List of Figures

Chapter One

Introduction

1.1 Nano Science

Nano science is one of the most interesting branches of physics. Recently large amount of research has focused in determining the properties and potential functions of nanomaterials. Nanomaterials show numerous exceptional and valuable properties which can be applied in the areas of life science, biology and medicine research [1].

Nanoparticles (NPs) are submicron particles with diameters ranging from 1 to 100 nm and made of inorganic or organic materials. As compared with bulk materials, NPs have many unique characteristics; although real uses of NPs in life sciences are still rarely found, great features of these materials propose a very good future for their use in this field [2].

The physics of magnetic nanoparticles systems is of special scientific interest, and has attracted much attention in recent years due to the potential for various applications, from technology to medicine [3].

Magnetic fields are widely used in technology. Magnetic nanoparticles (MNPs) are one of the types of NPs which exhibit some response to applying magnetic field. In this regard, MNPs have various unique magnetic properties including superparamagnetic, high magnetic susceptibility, low Curie temperature, etc.

In addition, these materials have been used in various industrial, medical, and environmental domains.

The change of magnetic properties can be done by changing Nano structure. Magnetic properties of nanoparticles the behavior of substances under an influence of an external magnetic field is determined by two factors susceptibility and permeability.

Susceptibility (χ) describes the magnetization level (M) of a material in the presence of an external magnetic field (H). The permeability indicates the magnetic induction (B) change induced by an external magnetic field (B= μH), the matter with high permeability reveals a low resistance in reaction to magnetic field. The size of magnetic nanoparticle, however, is comparable to the size of a magnetic domain, which results in a completely novel phenomenology with respect to bulk magnetic materials. In particular, the properties of the valence electrons of atoms (which are mainly responsible of the magnetic character of atoms and solids) change as they become part of small metallic particle and start to delocalize. Thus, their magnetic properties are very sensitive to size, composition, and local atomic

environment, showing a wide variety of intriguing phenomena. This rich variety of behavior can be understood in general terms as a rising from the reduced a verge coordination per atom; the quantum size effect (the wave function of electrons changes when they are confined to dimensions comparable with their wavelength, so that the continuous bulk bands spilt up in to discrete levels); and modified collective electron behavior such as screening and charge spill-out from the surface [4].

The synthesis of magnetic spinel ferrites at the nanoscale is a field of intense study, because the mesoscopic properties enable their novel applications. Spinel nanoparticles have a promising role because of their extraordinary properties compared with those of micro and macro scale particles [5].

1.2 Research Problems:-

Magnetic materials are widely used in technology, thus an extensive research is needed to produce materials having new magnetic properties. This can be done by using nanoscience to produce nanomagnetic materials.

1.3 Objectives:-

1.3.1 General Objective

The aim of this work is to study how the sizes of Nano particles affect on optical, electrical and magnetic properties of nanoparticles.

1.3.2 Specific Objectives

The specific objectives are:-

1-To study the properties and to check the Nano structure of magnetic Nano particles one uses the scanning electron microscope (SEM).

2-The study of optical properties of Fe_3O_4 and Ni_2O_3 nanoparticles is done by using UV photospectrometer.

3-The magnetic permeability can also be studied by finding refractive index.

4-The energy gap and absorption can be studied by using UV photospectrometer.

4-The study of Crystal structure of Fe_3O_4 and Ni_2O_3 nanoparticles is done by using x-ray Diffract meter (XRD).

1.4 Layout of the Thesis

Chapter one is the introduction which is concerned with the research problem, objectives and materials. Chapter two is about theoretical background that includes crystal structure of solid, thin film, nanomaterials and their properties. Chapter three is about previous studies while chapter four is devoted for experiment details (materials and method), discussion and results. Chapter five is concerned with conclusion and recommendations.

Chapter TWO
Theoretical Background

2.1 Introduction

The Nano material properties need enough background and about the crystal structure, thin film techniques, optical and magnetic properties.

2.2 The Structure of Crystalline Solids

Solid materials may be classified according to the regularity with which atoms or ions are arranged with respect to one another.

Material is one in which the atoms are situated in a repeating or periodic array over large atomic distances; that is, long range order exists, such that upon solidification, the atoms will position themselves in a repetitive three-dimensional pattern, in which each atom is bonded to its nearest-neighbour atoms.

Some of the properties of crystalline solids depend on the crystal structure of the material, the manner in which atoms, ions, or molecules are spatially arranged. There is an extremely large number of different crystal structures all having long-range atomic order; these vary from relatively simple structures for metals to exceedingly complex ones, as displayed by some of the ceramic and polymeric materials.

Sometimes the term lattice is used in the context of crystal structures; in this sense lattice means a three-dimensional array of points coinciding with atom positions.

The atomic order in crystalline solids indicates that small groups of atoms form a repetitive pattern. Thus, in describing crystal structures, it is often convenient to subdivide the structure into small repeat entities called unit cells.

A unit cell is chosen to represent the symmetry of the crystal structure, wherein all the atom positions in the crystal may be generated by translations of the unit cell integral distances along each of its edges. Thus, the unit cell is the basic structural unit or building block of the crystal structure and defines the crystal structure by virtue of its geometry and the atom positions within [6].

2.2.1 Metallic crystal structures

There are three relatively simple crystal structures are found for most of the common metals:-

2.2.1.1 The Face-Centred Cubic Crystal Structure

The crystal structure found for many metals has a unit cell of cubic geometry, with atoms located at each of the corners and the centres of all the cube faces. It is aptly called the face-centred cubic (FCC) crystal structure as shown in figure (2.1).
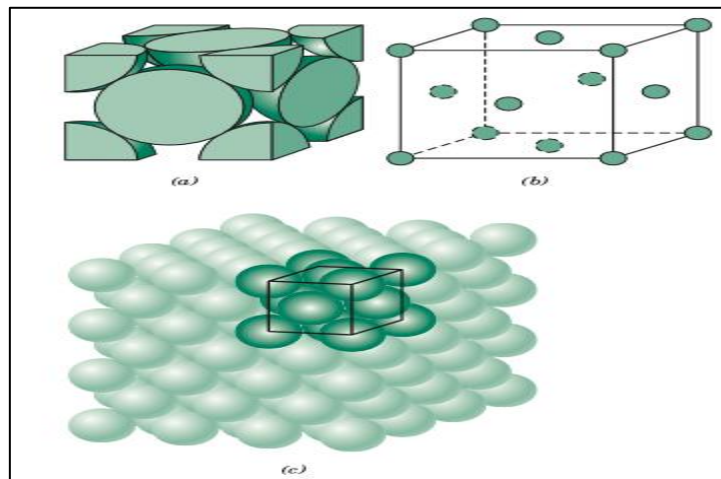
Figure (2.1) for the face centred cubic crystal structure, (a) a hard sphere unit cell representation, (b) a reduced-sphere unit cell, and (c) an aggregate of many atoms.

2.2.1.2The Body-Centred Cubic Crystal Structure

Another common metallic crystal structure also has a cubic unit cell with atoms located at all eight corners and a single atom at the cube centre. This is called a body-centred cubic (BCC) crystal structure as shown in figure (2.2).
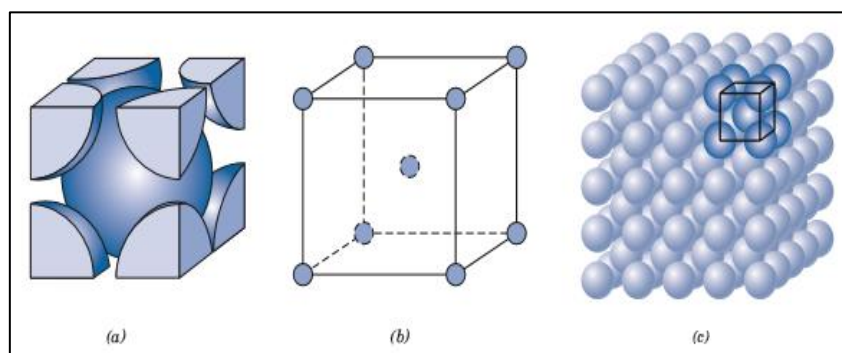
Figure (2.2) For the body-centred cubic crystal structure, (a) a hard-sphere unit cell representation, (b) a reduced-sphere unit cell, and (c) an aggregate of many atoms

2.2.1.3The Hexagonal Close-Packed Crystal Structure

Not all metals have unit cells with cubic symmetry; the final common metallic crystal structure to be discussed has a unit cell that is hexagonal. The term hexagonal close-packed brief as (HCP) which was shown in figure (2.3).

The top and bottom faces of the unit cell consist of six atoms that form regular hexagons and surround a single atom in the centre [7].
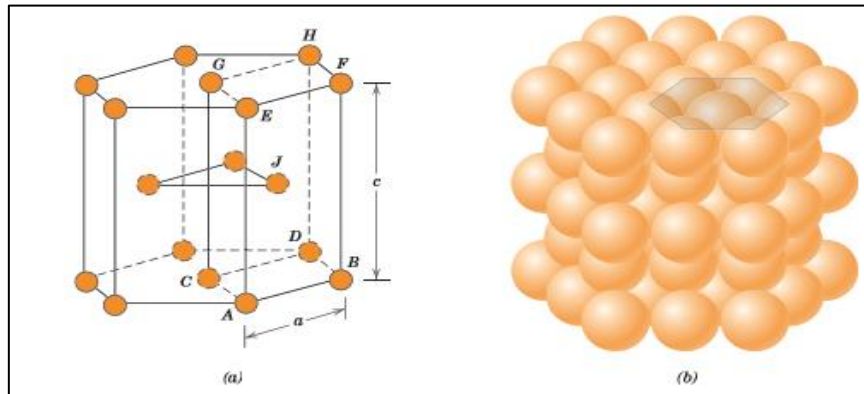
Figure (2.3) for the hexagonal close-packed crystal structure, (a) a reduced-sphere unit cell (a and c represent the short and long edge lengths, respectively), and (b) an aggregate of many atoms.

2.2.2 Crystal System

The unit cell geometry is completely defined in terms of six parameters: the three edge lengths a, b, and c, and the three interaxial angles α, β, and γ. and are sometimes termed the lattice parameters of a crystal structure.

On this basis there are seven different possible combinations of a, b, and c, and α, β, and γ, each of which represents a distinct crystal system. These seven crystal systems are cubic, tetragonal, hexagonal, orthorhombic, rhombohedral, monoclinic, and triclinic.
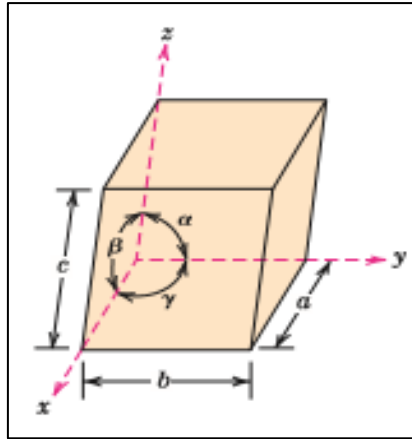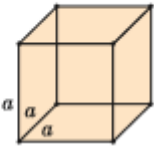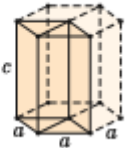
Figure (2.4) A unit cell with x, y, and z coordinate axes, showing axial lengths (a, b, and c) and interaxial angles (α, β, and γ)

Table 2-1   Lattice Parameter Relationships and Figures Showing Unit Cell Geometries for the two Crystal Systems

Crystal System	Axial Relationships	Interaxial Angles	Unit Cell Geometry
Cubic	$a = b = c$	$\alpha = \beta = \gamma = 90°$	
Hexagonal	$a = b \neq c$	$\alpha = \beta = 90°, \gamma = 120°$	

2.2.3 Crystallographic planes (Miller indices)

The orientations of planes for a crystal structure are represented in a similar manner. Again, the unit cell is the basis, with the three-axis coordinate system. In all but the hexagonal crystal system, crystallographic planes are specified by three Miller indices as (h k l). Any two planes parallel to each other are equivalent and have identical indices [8].
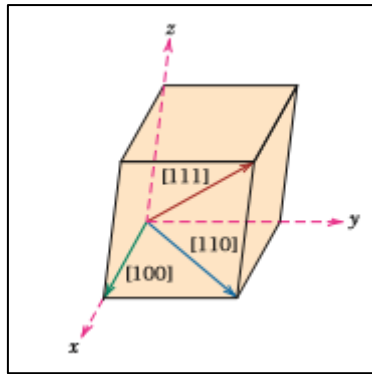
Figure (2.5) the [100], [110], and [111] directions within a unit cell.
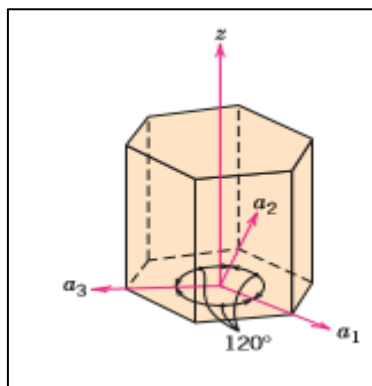
Figure (2.6) Coordinate axis system for a hexagonal unit cell (Miller–Bravais scheme).

2.3 Thin Film

A thin film is a layer of material ranging from fractions of a nanometre (monolayer) to several micrometres in thickness. The controlled synthesis of materials as thin films (process referred to as deposition) is a fundamental step in many applications.

In addition to their applied interest, thin films play an important role in the development and study of materials with new and unique properties.

2.3.1 Deposition

The act of applying a thin film to a surface is thin-film deposition – any technique for depositing a thin film of material onto a substrate or onto previously deposited layers. "Thin" is a relative term, but most deposition techniques control layer thickness within a few tens of nanometres [9].

2.3.2 Deposition Techniques

Almost all of these deposition techniques can be broadly divided into two categories, namely

1- physical vapour deposition processes (PVD). The PVD processes include laser ablation, sputtering.

2- Chemical vapour deposition techniques (CVD), liquid phase epitaxy, sol-gel and metal organic deposition (MOD) and spin coating. There have been many extensive reviews on the deposition of epitaxial oxide films [10].

2.4 Nanomaterials

One new material class that has fascinating properties and tremendous technological promise is the nanomaterials. Nanomaterials may be any one of the four basic types—metals, ceramics, polymers, and composites. However, unlike these other materials, they are not distinguished on the basis of their chemistry, but rather, size; the Nano-prefix denotes that the dimensions of these structural entities are on the order of a nanometre (10^{-9} m) as a rule, less than 100 nanometres (equivalent to approximately 500 atom diameters). Prior to the advent of nanomaterials, the general procedure scientists used to understand the chemistry and physics of materials was to begin by studying large and complex structures, and then to investigate the fundamental building blocks of these structures that are smaller and simpler. This approach is sometimes termed "top-down" science. On the other hand, with the development of scanning probe microscopes, which permit observation of individual atoms and molecules, it has become possible to design and build new structures from their atomic level constituents, one atom or molecule at a time (i.e., "materials by design").This ability to carefully arrange atoms provides opportunities to develop mechanical, electrical, magnetic, and other properties that are not otherwise possible. We call this the "bottom-up" approach, and the study of the properties of these materials is termed nanotechnology. Some of the physical and chemical characteristics exhibited by matter may experience dramatic changes as particle size approaches atomic dimensions. For example, materials that are opaque in the macroscopic domain may become transparent on the nanoscale; some solids become liquids, chemically stable materials become combustible, and electrical insulators become conductors. Furthermore, properties may depend on size in this nanoscale domain. Some of these effects are quantum mechanical in origin; others are related to surface phenomena the proportion of atoms located on surface sites of a particle increases dramatically as its size decreases. Because of these unique and unusual properties, nanomaterials are finding niches in electronic, biomedical, sporting, energy production, and other industrial applications [11].

2.5 Techniques to Make Nanomaterials

Nanomaterials can be made using a wide variety of methods, which can be classified in two broad categories:-

(a) Top-down processes, in which material is removed from a larger scale object to create nanostructures (e.g., lithography, either using electron beams, ion beams or X-rays). Lithography is heavily used in the semiconductor processing industry to fabricate integrated circuits and optoelectronic components. Alternatively, the material can broke down into subsequently smaller particles, until the nanoscale is reached (high-energy ball milling). This process is widely used to fabricate nanomaterials in the form of powders.

(b) Bottom-up processes, in which building blocks (atoms, molecules) are assembled together into progressively larger structures until the nanoscale is reached.

2.6 Techniques to Study Nanomaterials

The multi- and cross-disciplinary character of Nanoscience is also reflected in the multitude of techniques that are required to unravel and understand the properties of nanomaterials. Given the extent of the subject, we will provide below only a brief overview of the essential techniques to study nanoparticles (NPs) [12].

2.6.1 X-Ray diffraction (XRD): Determination of crystal structures

Historically, much of our understanding regarding the atomic and molecular arrangements in solids has resulted from x-ray diffraction investigations; furthermore, x-rays are still very important in developing new materials.

X-rays are a form of electromagnetic radiation that have high energies and short wavelengths, wavelengths on the order of the atomic spacing for solids. When a beam of x-rays impinges on a solid material, a portion of this beam will be scattered in all directions by the electrons associated with each atom or ion that lies within the beam's path.

Consider the two parallel planes of atoms (A- A⁻ and B − B⁻). In Figure (2.7), which have the same h, k, and *l* Miller indices and are separated by the interplanar spacing d_{hkl}.

Now assume that a parallel, monochromatic, and coherent (in-phase) beam of x-rays of wavelength is incident on these two planes at an angle .Two rays in this beam, labelled 1 and 2, are scattered by atoms P and Q. Constructive interference of the scattered rays 1⁻and 2⁻ occurs also at an angle θ to the planes.
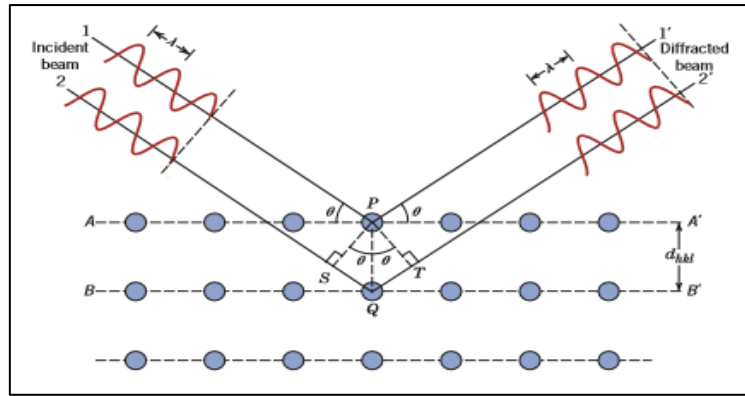
Figure (2.7) Diffraction of x-rays by planes of atoms (A- A⁻ and B - B⁻).

The diffract meter is an apparatus used to determine the angles at which diffraction occurs for powdered specimens.

One of the primary uses of x-ray diffract meter is for the determination of crystal structure. The unit cell size and geometry may be resolved from the angular positions of the diffraction peaks, whereas arrangement of atoms within the unit cell is associated with the relative intensities of these peaks. X-rays, as well as electron and neutron beams, are also used in other types of material investigations.

X-ray diffraction (XRD) is a powerful non-destructive technique for characterizing crystalline materials. It provides information on structures, phases, preferred crystal orientations (texture), and other structural parameters, such as average grain size, crystalline, strain, and crystal defects. X-ray diffraction peaks are produced by constructive interference of a monochromatic beam of X-rays scattered at specific angles from each set of lattice planes in a sample. The peak intensities are determined by the distribution of atoms within the lattice. Consequently, the X-ray diffraction pattern is the fingerprint of periodic atomic arrangements in a given material. This review summarizes the scientific trends associated with the rapid development of the technique of X-ray diffraction over the past five years pertaining to the field of pharmaceutical industry, forensic science, geological applications, microelectronics and glass industry, as well as in corrosion analysis [13].

2.6.2 Scanning Electron Microscopes (SEM)

A more recent and extremely useful investigative tool is the scanning electron microscope (SEM).The surface of a specimen to be examined is scanned with an electron beam, and the reflected (or back-scattered) beam of electrons is collected, then displayed at the same scanning rate on a cathode ray tube (similar to a CRT television screen). The image on the screen, which may be photographed, represents the surface features of the specimen. The

surface may or may not be polished and etched, but it must be electrically conductive; a very thin metallic surface coating must be applied to nonconductive materials. Magnifications ranging from 10 to in excess of 50,000 times are possible, as are also very great depths of field. Accessory equipment permits qualitative and semi quantitative analysis of the elemental composition of much localized surface areas [14].

2.6.3 UV-VIS Spectrophotometer

Ultraviolet-visible spectroscopy is considered an important tool in analytical chemistry. In fact, this is one of the most commonly used techniques in clinical as well as chemical laboratories. This tool is used for the qualitative analysis and identification of chemicals. However, its main use is for the quantitative determination of different organic and inorganic compounds in solution.

Basically, spectroscopy is related to the interaction of light with matter. As light is absorbed by matter, the result is an increase in the energy content of the atoms or molecules.

The absorption of visible light or ultraviolet light by a chemical compound will produce a distinct spectrum.

When ultraviolet radiations are absorbed, this results in the excitation of the electrons from the ground state towards a higher energy state. The theory revolving around this concept states that the energy from the absorbed ultraviolet radiation is actually equal to the energy difference between the higher energy state and the ground state [15].

2.7 Optical Properties

Optical property refers to a material's response to exposure to electromagnetic radiation and, in particular, to visible light. This section first discusses some of the basic principles and concepts relating to the nature of electromagnetic radiation and its possible interactions with solid materials. Next to be explored are the optical behaviours of metallic and non-metallic materials in terms of their absorption, reflection, and transmission characteristics.

2.7.1 Electromagnetic Radiation

Electromagnetic radiation is considered to be wavelike, consisting of electric and magnetic field components that are perpendicular to each other and also to the direction of propagation (Figure 2.8).
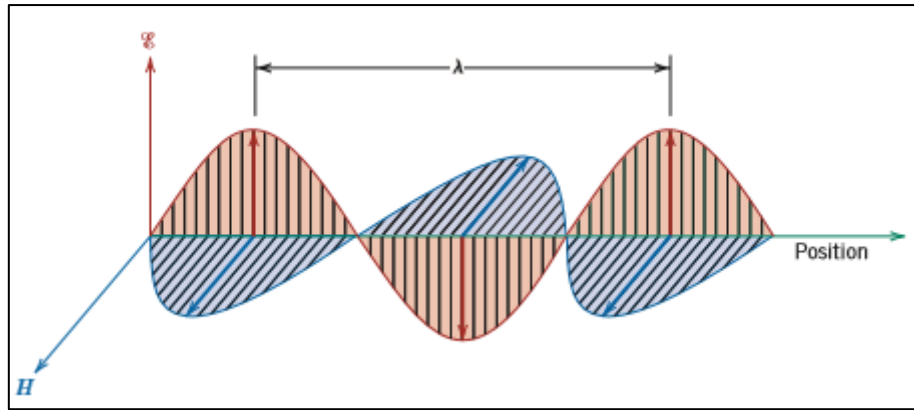
Figure (2.8) an electromagnetic wave showing electric field E and magnetic field H components, and the wavelength λ.

All electromagnetic radiation traverses a vacuum at the same velocity (3×10^8 m/s). This velocity, c, is related to the electric permittivity of a vacuum ε_0 and the magnetic permeability of a vacuum μ_0 through the relation

$$C = \frac{1}{\sqrt{\varepsilon_0 \mu_0}}$$ (2.1)

Thus, there is an association between the electromagnetic constant c and these electrical and magnetic constants. The figure (2.9) present electromagnetic radiation with wavelength.
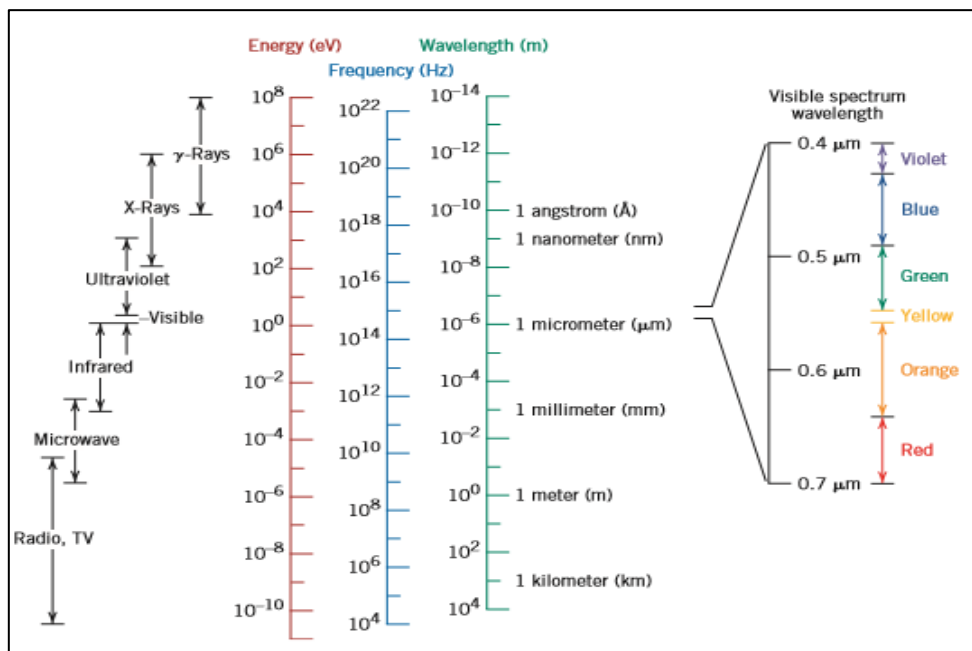
Figure (2.9) the spectrum of electromagnetic radiation, including wavelength ranges for the various colours in the visible spectrum

Furthermore, the frequency ν and the wavelength λ of the electromagnetic radiation are a function of velocity according to

$$C = \lambda \, \nu \tag{2.2}$$

Sometimes it is more convenient to view electromagnetic radiation from a quantum-mechanical perspective, in which the radiation, rather than consisting of waves, is composed of groups or packets of energy, which are called photons. The energy E of a photon is said to be quantized, or can only have specific values, defined by the relationship [16].

$$E = h\nu = \frac{h\,c}{\lambda} \tag{2.3}$$

Where h is a universal constant called Planck's constant, which has a value of 6.63×10^{-34} J.S

2.7.2 Light Interactions with Solids

When light proceeds from one medium into another (e.g., from air into a solid substance), several things happen. Some of the light radiation may be transmitted through the medium, some will be absorbed, and some will be reflected at the interface between the two media.

The intensity I_0 of the beam incident to the surface of the solid medium must equal the sum of the intensities of the transmitted, absorbed, and reflected beams, denoted as I_T, I_A, and I_R, respectively,

$$I_0 = I_T + I_A + I_R \tag{2.4}$$

An alternate form of Equation 2.4 is

$$T + A + R = 1 \tag{2.5}$$

where T, A, and R represent, respectively, the transmissivity (I_T/I_0), absorptivity (I_A/I_0),and reflectivity (I_R/I_0),or the fractions of incident light that are transmitted, absorbed, and reflected by a material; their sum must equal unity, because all the incident light is either transmitted, absorbed, or reflected [17].

2.7.3 Refraction

Light that is transmitted into the interior of transparent materials experiences a decrease in velocity, and, as a result, is bent at the interface; this phenomenon is termed refraction.

The index of refraction n of a material is defined as the ratio of the velocity in a vacuum c to the velocity in the medium v or

$$n = \frac{c}{v} \tag{2.6}$$

An equivalent expression gives the velocity of light v in a medium as

$$v = \frac{1}{\sqrt{\varepsilon\,\mu}} \qquad (2.7)$$

Where ε and μ are, respectively, the permittivity and permeability of the particular substance.

From the equation (2-6), we have

$$n = \frac{c}{v} = \frac{\sqrt{\varepsilon\,\mu}}{\sqrt{\varepsilon_0\mu_0}} = \sqrt{\varepsilon_r\mu_r} \qquad (2.8)$$

Where ε_r and μ_r are the dielectric constant and the relative magnetic permeability, respectively. Because most substances are only slightly magnetic, $\mu_r \cong 1$

$$n \cong \sqrt{\varepsilon_r} \qquad (2.9)$$

Thus, for transparent materials, there is a relation between the index of refraction and the dielectric constant. The phenomenon of refraction is related to electronic polarization at the relatively high frequencies for visible light; thus, the electronic component of the dielectric constant may be determined from index of refraction measurements using Equation (2.9). Because the retardation of electromagnetic radiation in a medium results from electronic polarization, the size of the constituent atoms or ions has a considerable influence on the magnitude of this effect generally, the larger an atom or ion, the greater the electronic polarization ,the slower the velocity, and the greater the index of refraction.

2.7.4 Reflection

When light radiation passes from one medium into another having a different index of refraction, some of the light is scattered at the interface between the two media even if both are transparent.

The reflectivity represents the fraction of the incident light that is reflected at the interface

$$R = \frac{I_R}{I_0} \qquad (2.10)$$

Where I_0 and I_R are the intensities of the incident and reflected beams, respectively. If the light is normal (or perpendicular) to the interface, then

$$R = \left(\frac{n_2 - n_1}{n_2 + n_1}\right)^2 \qquad (2.11)$$

Where n_1 and n_2 are the indices of refraction of the two media.

When light is transmitted from a vacuum or air into a solid s, then

$$R = \left(\frac{n_s - 1}{n_s + 1}\right)^2 \qquad (2.12)$$

Because the index of refraction of air is very nearly unity.

2.7.5 Absorption

Absorption of a photon of light may occur by the promotion or excitation of an electron from the nearly filled valence band, across the band gap, and into an empty state within the conduction band, as demonstrated in Figure 2.10a; a free electron in the conduction band and a hole in the valence band are created.

These excitations with the accompanying absorption can take place only if the photon energy is greater than that of the band gap E_g that is, if

$$h\,\nu > E_g \tag{2.13}$$

Or, in terms of wavelength

$$\frac{h\,c}{\lambda} > E_g \tag{2.14}$$

The minimum wavelength for visible light, λ (min), is about 0.4 µm, and because $C = 3 \times 10^8$ m/s and $h = 4.13 \times 10^{-15}$ eV.S, the maximum band gap energy E_g (max) for which absorption of visible light is possible is just

$$E_g \text{ (max)} = \frac{h\,c}{\lambda(\text{min})} = \frac{(4.13 \times 10^{-15} \text{ eV.S})(3 \times 10^8 \text{ m/s })}{4 \times 10^{-7}\ m} = 3.1\ eV \tag{2.15}$$
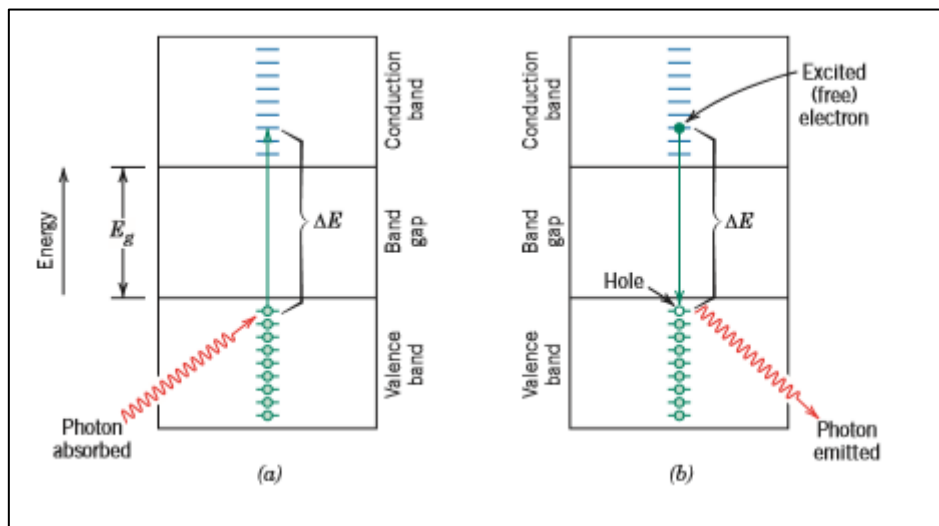
Figure (2.10) (a) Mechanism of photon absorption for non-metallic materials in which an electron is excited across the band gap, leaving behind a hole in the valence band. The energy of the photon absorbed is E, which is necessarily greater than the band gap energy E_g.

(b) Emission of a photon of light by a direct electron transition across the band gap.

Or, no visible light is absorbed by non-metallic materials having band gap energies greater than about 3.1 eV; these materials, if of high purity, will appear transparent and colourless.

On the other hand, the maximum wavelength for visible light, (max), is about 0.7μm; computation of the minimum band gap energy E_g(min) for which there is absorption of visible light is according to

$$E_g \text{ (min)} = \frac{h c}{\lambda(\text{max})} = \frac{(4.13 \times 10^{-15} \text{ eV.S})(3 \times 10^8 \text{ m/s})}{7 \times 10^{-7} \text{ m}} = 1.8 \text{ eV} \tag{2.16}$$

This result means that all visible light is absorbed by valence-band-to-conduction band electron transitions for semiconducting materials that have band gap energies less than about 1.8 eV; thus, these materials are opaque. Only a portion of the visible spectrum is absorbed by materials having band gap energies between 1.8 and 3.1 eV; consequently, these materials appear coloured.

Every non-metallic material becomes opaque at some wavelength, which depends on the magnitude of its E_g.

The intensity of the net absorbed radiation is dependent on the character of the medium as well as the path length within. The intensity of transmitted or non-absorbed radiation I_T continuously decreases with distance x that the light traverses:

$$I_T = I_0 e^{-\beta x} \tag{2.17}$$

Where is the intensity of the non-reflected incident radiation and β the absorption coefficient (in mm^{-1}), is characteristic of the particular material; furthermore, β varies with wavelength of the incident radiation. The distance parameter x is measured from the incident surface into the material. Materials that have large β values are considered highly absorptive.
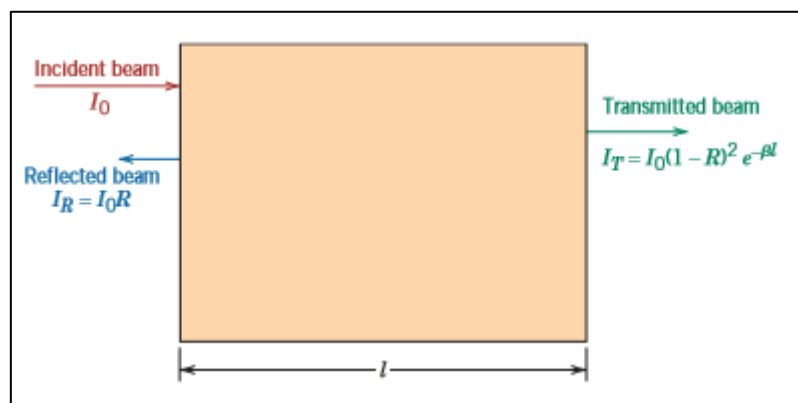
Figure (2.11) the transmission of light through a transparent medium for which there is reflection at front and back faces, as well as absorption within the medium.

2.7.6 Transmission

The phenomena of absorption, reflection, and transmission may be applied to the passage of light through a transparent solid, as shown in Figure 2.11. For an incident beam of intensity I_0 that impinges on the front surface of a specimen of thickness l and absorption coefficient β, the transmitted intensity at the back face I_T is

$$I_T = I_0 (1 - R)^2 e^{-\beta l} \tag{2.18}$$

Where R is the reflectance.

Thus, the fraction of incident light that is transmitted through a transparent material depends on the losses that are incurred by absorption and reflection. Again, the sum of the reflectivity R, absorptivity A, and transmissivity T, is unity according to Equation (2.18) [18].

2.8 Magnetic Properties

Magnetism, the phenomenon by which materials assert an attractive or repulsive force or influence on other materials, has been known for thousands of years.

However, the underlying principles and mechanisms that explain the magnetic phenomenon are complex and subtle, and their understanding has eluded scientists until relatively recent times. Many of our modern technological devices rely on magnetism and magnetic materials; these include electrical power generators and transformers, electric motors, radio, television, telephones, computers, and components of sound and video reproduction systems. Iron, some steels, and the naturally occurring mineral lodestone are well-known examples of materials that exhibit magnetic properties. Not so familiar, however, is the fact that all substances are influenced to one degree or another by the presence of a magnetic field. This chapter provides a brief description of the origin of magnetic fields and discusses the various magnetic field vectors and magnetic parameters; the phenomena of diamagnetism, paramagnetism, ferromagnetism, and ferrimagnetism; some of the different magnetic materials; and the phenomenon of superconductivity [19].

2.8.1 Magnetic Dipoles

Magnetic forces are generated by moving electrically charged particles; these magnetic forces are in addition to any electrostatic forces that may prevail. Many times it is convenient to think of magnetic forces in terms of fields. Imaginary lines of force may be drawn to indicate the direction of the force at positions in the vicinity of the field source. The magnetic field distributions as indicated by lines of force are shown for a current loop and also a bar magnet in Figure 2.12. Magnetic dipoles are found to exist in magnetic materials, which, in some respects, are analogous to electric dipoles. Magnetic dipoles may be thought of as small bar

magnets composed of north and south poles instead of positive and negative electric charges. In the present discussion, magnetic dipole moments are represented by arrows, as shown in Figure 2.13. Magnetic dipoles are influenced by magnetic fields in a manner similar to the way in which electric dipoles are affected by electric fields. Within a magnetic field, the force of the field itself exerts a torque that tends to orient the dipoles with the field. A familiar example is the way in which a magnetic compass needle lines up with the earth's magnetic field.
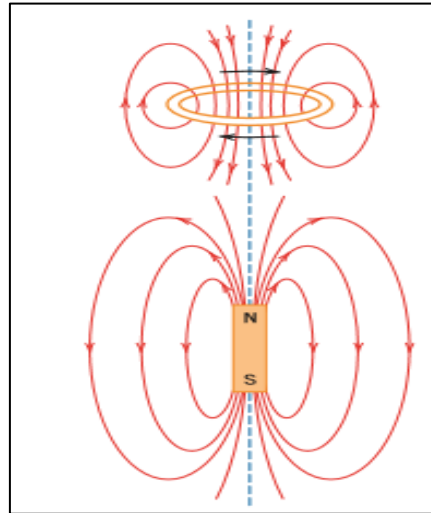
Figure (2.12) Magnetic field lines of force around a current loop and a bar magnet.

2.8.2 Magnetic Field Vectors

Before discussing the origin of magnetic moments in solid materials, we describe magnetic behaviour in terms of several field vectors. The externally applied magnetic field, sometimes called the magnetic field strength, is designated by H. If the magnetic field is generated by means of a cylindrical coil (or solenoid) consisting of N closely spaced turns, having a length *l*, and carrying a current of magnitude I, then (Magnetic field strength within a coil dependence on number of turns, applied current, and coil length)

$$H = \frac{NI}{l} \qquad\qquad (2.19)$$

A schematic diagram of such an arrangement is shown in Figure 2.14a the magnetic field that is generated by the current loop and the bar magnet in Figure 2.12 is an H field. The units of H are ampere-turns per meter, or just amperes per meter. The magnetic induction, or magnetic flux density, denoted by B, represents the magnitude of the internal field strength within a substance that is subjected to an H field. The units for B are teslas [or webers per

square meter (Wb/m^2)]. Both B and H are field vectors, being characterized not only by magnitude, but also by direction in space.
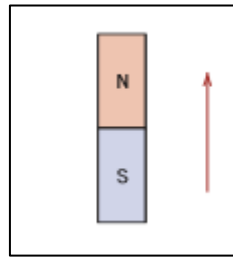
Figure (2.13) the magnetic moment as designated by an arrow.
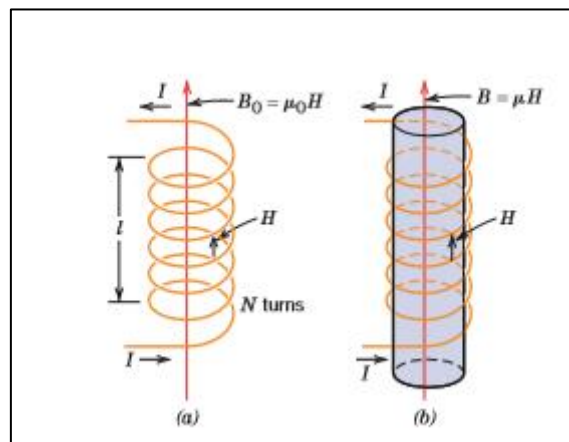
Figure (2.14) (a) The magnetic field H as generated by a cylindrical coil is dependent on the current I, the number of turns N, and the coil length l, according to Equation 2.19. The magnetic flux density B$_0$ in the presence of a vacuum is equal to μ_0 H, where μ_0 is the permeability of a vacuum, $4\pi \times 10^{-7}$ H/m.

(b) The magnetic flux density B within a solid material is equal to H, where is the permeability of the solid material.

The magnetic field strength and flux density are related according to (Magnetic flux density in a material dependence on permeability and magnetic field strength)

$$B = \mu\, H \tag{2.20}$$

The parameter is called the permeability, which is a property of the specific medium through which the H field passes and in which B is measured, as illustrated in Figure 2.14b. The permeability has dimensions of webers per ampere-meter (Wb/A m) or henries per meter (H/m).

In a vacuum, Magnetic flux density

$$B_0 = \mu_0\, H \tag{2.21}$$

Where μ_0 is the permeability of a vacuum, a universal constant, which has a value of $4\pi \times 10^{-7}$ (1.257×10^{-6}) H/m. The parameter B_0 represents the flux density within a vacuum as demonstrated in Figure 2.14 a. Several parameters may be used to describe the magnetic properties of solids. One of these is the ratio of the permeability in a material to the permeability in a vacuum, or relative permeability

$$\mu_r = \frac{\mu}{\mu_0} \tag{2.22}$$

Where μ_r is called the relative permeability, which is unit less.

The permeability or relative permeability of a material is a measure of the degree to which the material can be magnetized, or the ease with which a B field can be induced in the presence of an external H field.

Another field quantity, M, called the magnetization of the solid, is defined by the expression (Magnetic flux density as a function of magnetic field strength and magnetization of a material)

$$B = \mu_0 H + \mu_0 M \tag{2.23}$$

In the presence of an H field, the magnetic moments within a material tend to become aligned with the field and to reinforce it by virtue of their magnetic fields; the term in Equation 2-23 is a measure of this contribution.

The magnitude of M is proportional to the applied field as follows:

(Magnetization of a material dependence on susceptibility and magnetic field strength)

$$M = \chi_m H \tag{2.24}$$

And χ_m is called the magnetic susceptibility, which is unit less. The magnetic susceptibility and the relative permeability are related as follows:

(Relationship between magnetic susceptibility and relative permeability)

$$\chi_m = \mu_r - 1 \tag{2.25}$$

2.8.3 Origins of Magnetic Moments

The macroscopic magnetic properties of materials are a consequence of magnetic moments associated with individual electrons. Some of these concepts are relatively complex and involve some quantum-mechanical principles beyond the scope of this discussion; consequently, simplifications have been made and some of the details omitted. Each electron in an atom has magnetic moments that originate from two sources. One is related to its orbital motion around the nucleus; being a moving charge
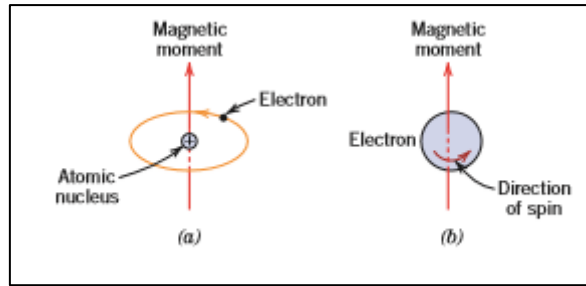
Figure (2.15) Demonstration of the magnetic moment associated with (a) an orbiting electron and (b) a spinning electron

an electron may be considered to be a small current loop, generating a very small magnetic field, and having a magnetic moment along its axis of rotation, as schematically illustrated in Figure 2.15 a. Each electron may also be thought of as spinning around an axis; the other magnetic moment originates from this electron spin, which is directed along the spin axis as shown in Figure 2.15b.Spin magnetic moments may be only in an "up" direction or in an antiparallel "down" direction. Thus each electron in an atom may be thought of as being a small magnet having permanent orbital and spin magnetic moments.

2.8.4 Bohr magneton

The most fundamental magnetic moment is the Bohr magnetonμ_B, which is of magnitude 9.27×10^{-24} Am^2. For each electron in an atom the spin magnetic moment is $\pm\mu_B$ (plus for spin up, minus for spin down).

In each individual atom, orbital moments of some electron pairs cancel each other; this also holds for the spin moments. For example, the spin moment of an electron with spin up will cancel that of one with spin down. The net magnetic moment, then, for an atom is just the sum of the magnetic moments of each of the constituent electrons, including both orbital and spin contributions, and taking into account moment cancellation. For an atom having completely filled electron shells or subshells, when all electrons are considered, there is total cancellation of both orbital and spin moments. Thus materials composed of atoms having completely filled electron shells are not capable of being permanently magnetized. This category includes the inert gases (He, Ne, Ar, etc.) as well as some ionic materials. The types of magnetism include diamagnetism, paramagnetism, and ferromagnetism; in addition, antiferromagnetic and ferrimagnetism are considered to be subclasses of ferromagnetism. All materials exhibit at least one of these types, and the behaviour depends on the response of electron and atomic magnetic dipoles to the application of an externally applied magnetic field [20].

2.8.5 Types of Magnetic materials

There are some magnetic materials such as:-

2.8.5.1 Diamagnetism and paramagnetism

Diamagnetism is a very weak form of magnetism that is non-permanent and persists only while an external field is being applied. It is induced by a change in the orbital motion of electrons due to an applied magnetic field. The magnitude of the induced magnetic moment is extremely small, and in a direction opposite to that of the applied field.

Thus, the relative permeability µr is less than unity (however, only very slightly), and the magnetic susceptibility is negative; that is, the magnitude of the B field within a diamagnetic solid is less than that in a vacuum. The volume susceptibility χ_m for diamagnetic solid materials is on the order of $- 10^{-5}$. When placed between the poles of a strong electromagnet, diamagnetic materials are attracted toward regions where the field is weak.
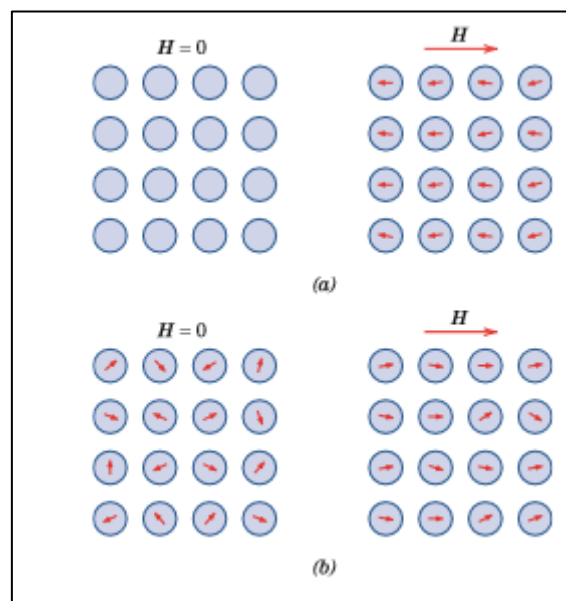
Figure (2.16) (a) the atomic dipole configuration for a diamagnetic material with and without a magnetic field. In the absence of an external field, no dipoles exist; in the presence of a field, dipoles are induced that are aligned opposite to the field direction. (b) Atomic dipole configuration with and without an external magnetic field for a paramagnetic material.

Figure 2.16a illustrates schematically the atomic magnetic dipole configurations for a diamagnetic material with and without an external field; here, the arrows represent atomic dipole moments, whereas for the preceding discussion, arrows denoted only electron moments. The dependence of B on the external field H for a material that exhibits diamagnetic behaviour is presented in Figure 2-17 Table 2.2 gives the susceptibilities of several diamagnetic materials. Diamagnetism is found in all materials, but because it is so weak, it can be observed only when other types of magnetism are totally absent.

This form of magnetism is of no practical importance. For some solid materials, each atom possesses a permanent dipole moment by virtue of incomplete cancellation of electron spin and/or orbital magnetic moments. In the absence of an external magnetic field, the orientations of these atomic magnetic moments are random, such that a piece of material possesses no net macroscopic magnetization. These atomic dipoles are free to rotate, and paramagnetism results when they preferentially align, by rotation, with an external field as shown in Figure 2-16b. These magnetic dipoles are acted on individually with no mutual
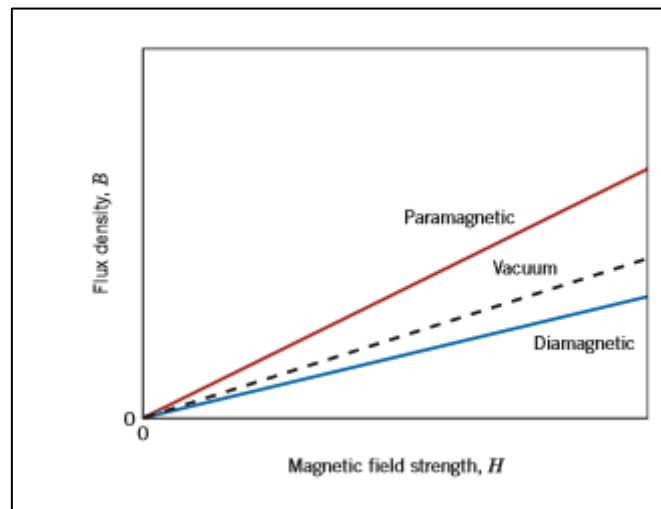
Figure (2.17) Schematic representation of the flux density B versus the magnetic field strength H for diamagnetic and paramagnetic materials.

Diamagnetics		Paramagnetics	
Material	Susceptibility χ_m (volume) (SI units)	Material	Susceptibility χ_m (volume) (SI units)
Aluminum oxide	-1.81×10^{-5}	Aluminum	2.07×10^{-5}
Copper	-0.96×10^{-5}	Chromium	3.13×10^{-4}
Gold	-3.44×10^{-5}	Chromium chloride	1.51×10^{-3}
Mercury	-2.85×10^{-5}	Manganese sulfate	3.70×10^{-3}
Silicon	-0.41×10^{-5}	Molybdenum	1.19×10^{-4}
Silver	-2.38×10^{-5}	Sodium	8.48×10^{-6}
Sodium chloride	-1.41×10^{-5}	Titanium	1.81×10^{-4}
Zinc	-1.56×10^{-5}	Zirconium	1.09×10^{-4}

Table 2.2 Room-Temperature Magnetic Susceptibilities for Diamagnetic and Paramagnetic Materials

Interaction between adjacent dipoles. Inasmuch as the dipoles align with the external field, they enhance it, giving rise to a relative permeability μr that is greater than unity, and to a relatively small but positive magnetic susceptibility.

Susceptibilities for paramagnetic materials range from about 10^{-5} to 10^{-2} (Table 20.2).A schematic B-versus-H curve for a paramagnetic material is also shown in Figure 20.6. Both diamagnetic and paramagnetic materials are considered nonmagnetic because they exhibit magnetization only when in the presence of an external field. Also, for both, the flux density B within them is almost the same as it would be in a vacuum.

2.8.5.2 Ferromagnetism

Certain metallic materials possess a permanent magnetic moment in the absence of an external field, and manifest very large and permanent magnetizations. These are the characteristics of ferromagnetism, and they are displayed by the transition metals iron (As BCC α - ferrite), cobalt, nickel, and some of the rare earth metals such as gadolinium (Gd). Magnetic susceptibilities as high as 10^6 are possible for ferromagnetic materials. Consequently, $H \ll M$ and from Equation 2-23 we write (For a ferromagnetic material, relationship between magnetic flux density and magnetization)

$$B \cong \mu_0 H \tag{2.26}$$

Permanent magnetic moments in ferromagnetic materials result from atomic magnetic moments due to un cancelled electron spins as a consequence of the electron structure.

There is also an orbital magnetic moment contribution that is small in comparison to the spin moment. Furthermore, in a ferromagnetic material, coupling interactions cause net spin magnetic moments of adjacent atoms to align with one another, even in the absence of an external field. This is schematically illustrated in Figure 2.18. The origin of these coupling

forces is not completely understood, but it is thought to arise from the electronic structure of the metal. This mutual spin alignment exists over relatively large-volume regions of the crystal called domains.

The maximum possible magnetization or saturation magnetization M_s, of a ferromagnetic material represents the magnetization that results when all the magnetic dipoles in a solid piece are mutually aligned with the external field; there is also a corresponding saturation flux density B_s.
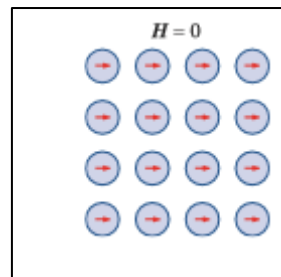
Figure (2.18) Schematic illustration of the mutual alignment of atomic dipoles for a ferromagnetic material, which will exist even in the absence of an external magnetic field.

The saturation magnetization is equal to the product of the net magnetic moment for each atom and the number of atoms present. For each of iron, cobalt, and nickel, the net magnetic moments per atom are 2.22, 1.72, and 0.60 Bohr magnetons, respectively.

2.8.5.3 *Antiferromagnetic*

This phenomenon of magnetic moment coupling between adjacent atoms or ions occurs in materials other than those that are ferromagnetic. In one such group, these coupling results in an antiparallel alignment; the alignment of the spin moments of neighbouring atoms or ions in exactly opposite directions is termed antiferromagnetic. Manganese oxide (MnO) is one material that displays this behaviour. Manganese oxide is a ceramic material that is ionic in character, having both Mn^{+2} and O^{-2} ions. No net magnetic moment is associated with the O^{-2} ions, because there is a total cancellation of both spin and orbital moments. However, the Mn^{+2} ions possess a net magnetic moment that is predominantly of spin origin. These Mn^{+2} ions are arrayed in the crystal structure such that the moments of adjacent ions are antiparallel. This arrangement is represented schematically in Figure 20.8. Obviously, the opposing magnetic moments cancel one another, and, as a consequence, the solid as a whole possesses no net magnetic moment.

2.8.5.4 Ferrimagnetism

Some ceramics also exhibit a permanent magnetization, termed ferrimagnetism. The macroscopic magnetic characteristics of Ferro magnets and ferrimagnetism are similar; the distinction lies in the source of the net magnetic moments. The principles of ferrimagnetism are illustrated with the cubic ferrites. These ionic materials may be represented by the chemical formula $MFe_2 O_4$, in which M represents any one of several metallic elements. The prototype ferrite is $Fe_3 O_4$, the mineral magnetite, sometimes called lodestone [21].

2.9 Electric Properties

2.9.1 Electrical conductivity

In most substances and over wide range of electric field strengths we find that the current density is proportional to the strength of electric field that causes it. The linear relation between current density J and field strength E is expressed by the equation

$$J = \sigma E \tag{2.26}$$

The factor σ is called the conductivity of the material; its value depends on the material; it is very large for metallic conductors, extremely small for good insulator. It may depend too on the physical state of the material [22].

2.9.2 Electric permittivity

Permittivity describes the amount of charge needed to generate one unit of electric flux in a particular medium. Accordingly, a charge will yield more electric flux in a medium with low permittivity than in a medium with high permittivity. Permittivity is the measure of a material's ability to store an electric field in the polarization of the medium.

The SI unit for permittivity is farad per meter (F/m or $F \cdot m^{-1}$).

The lowest possible permittivity is that of a vacuum. Vacuum permittivity, sometimes called the electric constant, is represented by ε_0 and has a value of approximately 8.85×10^{-12} F/m.

The permittivity of a dielectric medium is often represented by the ratio of its absolute permittivity to the electric constant. This dimensionless quantity is called the medium's relative permittivity, sometimes also called "permittivity".

Relative permittivity is also commonly referred to as the dielectric constant, a term which has been deprecated in physics and engineering as well as in chemistry [23].

2.9.3 Dielectric constant

Dielectric constant or relative permittivity is define by the relation

$$\varepsilon_r = \frac{\varepsilon}{\varepsilon_0} \qquad (2.27)$$

Which is greater than unity and represents the increase in charge storing capacity by insertion of the dielectric medium between the plates. The dielectric constant is one material property that is of prime consideration for capacitor design.

Imaginary part is always positive and represents loss factor or energy absorbed. The measurement of the real part of relative permittivity ε_r is generally done by measuring the charge in capacitance of a capacitor by the introduction of the dielectric between its electrodes [24].

The electric field E, displacement X, velocity V and acceleration a takes the

$$E = E_0 e^{-iwt} = E_m e^{i(kx-wt)}$$

$$x = x_0 e^{-iwt} \qquad v = \dot{x} = -iwx = v_0 e^{-iwt} \qquad a = \dot{v} = -iwv = -w^2 x \qquad (2.28)$$

The equation of motion of electrons or any charged particle is given by

$$m\ddot{x} = eE - \gamma_0 n_0 v \qquad (2.29)$$

Where n_0 is the medium number density hence

$$(\gamma_0 n_0 - iwm)v = eE$$

With γ_0 standing for the friction per particle. Therefore the velocity v is given

$$v = \frac{eE}{\gamma_0 n_0 - iwm} = \frac{e(\gamma_0 n_0 + iwm)E}{[\gamma_0^2 n_0^2 + w^2 m^2]} \qquad (2.30)$$

For very small mass m and high concentration n_0, such that

$$\gamma_0 n_0 > wm \qquad (2.31)$$

Equation (3) becomes

$$v = \left[\frac{e}{\gamma_0 n_0} + \frac{iwme}{\gamma_0^2 n_0^2}\right] E \qquad (2.32)$$

But the current density is given by

$$J = n\,e\,v = n\,e\,\frac{dx}{dt} = \frac{dnex}{dt} = \frac{dp}{dt} = x\frac{dE}{dt} = -iwxE = -iw(x_1 + ix_2)E$$

Where x represents electric susceptibility

 Using (5) gives

$$ne^2 = \left[\frac{1}{\gamma_0 n_0} + \frac{iwm}{\gamma_0^2 n_0^2}\right] E = [wx_2 - iwx_1]E \qquad (2.33)$$

Equating real and imaginary parts gives

$$x_1 = \frac{-m}{\gamma_0^2 \, n_0^2} \qquad\qquad x_2 = \frac{ne^2}{w\gamma_0 n_0} \tag{2.34}$$

The absorption coefficient is related to the complex wave number

$$k = k_1 + ik_2 \tag{2.35}$$

Where the intensity takes the form

$$I = |E|^2 = E \, m^2 \, e^{-k_2 x} = I_0 \, e^{-2k_2 x} = I_0 \, e^{-\alpha x} \tag{2.36}$$

Thus the absorption coefficient is given by

$$\alpha = 2k_2 \tag{2.37}$$

Using the relation between wave number with electric permittivity and magnetic permeability, one gets

$$k^2 = (k_1 + ik_2)^2 = k_1^2 - k_2^2 + 2k_1 k_2 i = \frac{w^2}{v^2} = w^2 \, \mu \, \varepsilon = w^2 \mu[\varepsilon_1 + i\varepsilon_2]$$

$$= w^2 \mu \, \varepsilon_1 + w^2 \mu \varepsilon_2 \tag{2.38}$$

Thus equation real and imaginary parts, yields

$$k_2 = \frac{w^2 \mu \varepsilon_2}{2k_1} = \frac{w^2 \mu \varepsilon_0 \, (1 + x_2)}{2k_1} \tag{2.39}$$

In view of equations (2-34) and (2-39), one gets

$$k_2 = \frac{w^2 \mu \varepsilon_0 \left(1 + \frac{ne^2}{w \, r_0 n_0}\right)}{k_1} \tag{2.40}$$

Thus according to equation (2-37) the absorption coefficient takes the form

$$\alpha = 2k_2 = \frac{2w^2 \mu \varepsilon_0}{k_1} \left(1 + \frac{ne^2}{w \, r_0 n_0}\right) \tag{2.41}$$

Chapter Three
Literature Review

3.1 Introduction

Nickel Oxide (NiO) is an important transition metal oxide with cubic lattice structure. Among the magnetic nanoparticles, fabrication of nickel nanoparticles is often more difficult than that of the other particles. This is because they are easily oxidized. To achieve pure nickel nanocrystals, numerous methods have been conducted in organic environments in order to prevent formation of hydroxide or oxidation. In the present work, we report the synthesis of NiO nanoparticles. Magnetic properties of NiO nanoparticles with different sizes and at different temperatures are compared. The phase structures, particle sizes and magnetic properties of NiO nanoparticles have been characterized by X-ray diffraction, TEM images and Vibrating Sample Magnetometer (VSM). One collected the experimental data reported in the literature that are concerned with magnetic and electric Nano materials smaller than that of the bulk matter. The magnetic properties are also affected by temperature as well as surface to volume ratio [25].

3.2 Magnetic Nano behaviour

The influence of the particle size on magnetic behaviours of nickel oxide nanoparticles (NiO NPs) was reported by Tayebe Razegh1 et.al NiO NPs with a uniform particle size were synthesized via a facile sol-gel method, and various sizes of NiO NPs (11, to 49 nm) were achieved by calcination at various temperatures (400, to 700 °C). X-ray diffraction (XRD) analysis revealed that increasing the calcination temperature increased the crystallite size. TEM observations and XRD analysis were used to determine the particle size of the NiO NPs. The field emission scanning electron microscopy (FESEM) and transmission electron microscopy (TEM) images showed flake-like morphologies, which consisted of interconnected nanoparticles with a porous channel. The magnetic properties of NiO NPs with different size were studied using vibrating sample magnetometer (VSM). The results suggested that the particle size plays an important role in magnetic property of NiO nanoparticles [26].

In the article of Ashwani Kumar Singh1 et.al, he proposed a facile one-step synthesis of Fe_3O_4 nanoparticles of different shapes and sizes by co-precipitation of $FeCl_2$ with piper dine. A careful investigation of TEM micrographs shows that the shape and size of nanoparticles can be tuned by varying the molarity of piper dines. XRD patterns match the standard phase of the spinal structure of Fe_3O_4 which confirms the formation of Fe_3O_4 nanoparticles.

Transmission electron microscopy reveals that molar concentration of $FeCl_2$ solution plays a significant role in determining the shape and size of Fe_3O_4 nanoparticles. Changes in the shape and sizes of Fe_3O_4 nanoparticles which are influenced by the molar concentration of $FeCl_2$ can easily be explained with the help of surface free energy minimization principle. Further, to study the magnetic behaviour of synthesized Fe_3O_4 nanoparticles, magnetization vs. magnetic field (M-H) and magnetization vs. temperature (M-T) measurements were carried out by using Physical Property Measurement System (PPMS). These results show systematic changes in various magnetic parameters like remnant magnetization (Mr), saturation magnetization (Ms), coercively (Hc), and blocking temperature (TB) with shapes and sizes of Fe_3O_4. These variations of magnetic properties of different shaped Fe_3O_4 nanoparticles can be explained with surface effect and finite size effect [27].

Recently, iron oxide nanoparticles (NPs) have attracted much consideration due to their unique properties, such as superparamagnetic, surface-to-volume ratio, greater surface area, and easy separation methodology. Various physical, chemical, and biological methods have been adopted to synthesize magnetic NPs with suitable surface chemistry. This done by Attarad Ali et.al summarizes the methods for the preparation of iron oxide NPs, size and morphology control, and magnetic properties with recent bioengineering, commercial, and industrial applications. Iron oxides exhibit great potential in the fields of life sciences such as biomedicine, agriculture, and environment. Nontoxic conduct and biocompatible applications of magnetic NPs can be enriched further by special surface coating with organic or inorganic molecules, including surfactants, drugs, proteins, starches, enzymes, antibodies, nucleotides, non-ionic detergents, and polyelectrolytes. Magnetic NPs can also be directed to an organ, tissue, or tumour using an external magnetic field for hyperthermia treatment of patients. Keeping in mind the current interest in iron NPs, this review is designed to report recent information from synthesis to characterization, and applications of iron NPs [28].

Another work done by Navin K et.al reports the synthesis of different particle size La0.7Sr0.3MnO$_3$ (LSMO) nanoparticles using non-aqueous sol gel synthesis route by calcination at temperatures 750°C, 850°C and 950°C. In the present work, the effect of particle size of LSMO nanoparticles on its structural, magnetic and transport properties has been studied in detail. The X-ray diffraction analysis confirms the formation of LSMO nanoparticles having rhombohedral ($R\bar{3}c$) structure with average particle size of 20nm, 22.5nm and 25.6nm. An increase in magnetization and decrease in coercively with increase in particle size is attributed to the magnetically disordered surface layer. The bifurcation in ZFC-FC magnetization indicates the possibility of spin glass like behaviour of the LSMO

nanoparticles. The effect of particle size on the resistivity and magneto resistance were studied by using different conduction mechanism for different temperature regions. The upturn in the ρ-T curve at lower temperatures was explained by using Kondo-like transport mechanism. The maximum LFMR achieved was 32.3% at a field of 1T at 10K for 20nm LSMO nanoparticle [29].

The dependence of the magnetic responsiveness on magnetite nanoparticle size has been studied by Bui TQ et.al. Mon disperse magnetite nanoparticles of 10 nm diameter were prepared by an ultrasonically enhanced co-precipitation procedure. A carboxyl-functionalised solvothermal approach was applied to synthesise magnetite nanoparticles with an average size of 30 nm. The particle sizes and their distribution have been determined by analysing TEM images and considering nanoparticle formation mechanisms. The magnetic characterisation revealed an inverse dependence between the magnetite nanoparticle size and its ability to respond to external magnetic fields, which was explained by the decrease of magnetic dipoles inside the tailing-away crystal of the magnetite nanoparticles. Negligible hysteresis with a small value of 5 Oe was found for the 10 nm nanoparticles, while the larger value of 80 Oe was determined for the 30 nm nanoparticles [30].

In the work of Zhang B et.al the experimental data found many new phenomena in nanomaterials compared with the counterparts of bulk materials, which are the reduction of atomic moments in clusters of Fe, Co, and Ni, decrease of Curie temperature in magnetic nanomaterials, oscillatory Curie temperature in ultrathin Ferro magnets, saturation magnetization decreases but coercive force increases as decreasing the Nano size in nanomaterials, and GMR (This is a project to get Nobel Prize), etc. It is interesting that the controversy of whether ballistic MR really exists was discussed in detail in the chapter [31].

Nanostructured magnetic systems form a new class of materials whose properties are of great interest to the fields of medicine, health, electro electronics, catalysis, and others. The superparamagnetic behaviour of nanoparticles (NPs) enables the delivery and manipulation of substances. In addition, these NPs are susceptible to derivatization/functionalization reactions that help to anchor agents such as, pharmaceuticals, therapeutic agents, biomarkers, and DNA to produce Nano therapeutic complexes and theranostic drugs. This chapter that was done by Soler MAG et.al present fundamental concepts of magnetism, including its manifestation in low-dimensional systems. It will also present the properties of the magnetic nanostructures formed by iron oxide-based colloids and the most applied chemical synthesis methods for the production of these NPs as well as for surface functionalization and film preparation. Complementarily, the discussion includes the major physic-chemical properties of the

complexes of superparamagnetic iron oxide particles and some of their most recent biomedical applications [32].

In the work of Sneha Upadhyay et.al studied the Structural and magnetic properties of chemically synthesized magnetite nanoparticles have been studied using X-ray diffraction, Transmission Electron Microscopy and Vibrating Sample Magnetometer. Magnetically the synthesized nanoparticles are ranging from superparamagnetic to multi domain state. Average crystallite size of the synthesized magnetite nanoparticles were determined using X-ray line broadening and are found to be in the range of 9–53 nm. On the other hand, the TEM images show that the size is ranging between 7.9 and 200 nm with the transition from spherical superparamagnetic particles to faceted cubic multi domain particles. Magnetic parameters of the samples show a strong dependence on average crystallite size [33].

In the work of GS Kumar et.al nickel ferrite nanostructures has drawn a great interest because of its inherent chemical, physical and electronic properties. In this study, we have synthesized rhombohedrum – like nickel ferrite nanostructure by a rapid microwave assisted combustion method using ethylene diamminetetraacetic acid as a chelating agent. X-ray diffraction, Fourier transform infrared spectrometer, transmission electron microscope and energy dispersive X-ray micro analyser were used to characterize the prepared sample. The magnetic behaviour was analysed by means of field dependent magnetization measurement which indicates that the prepared sample exhibits a soft ferromagnetic nature with saturation magnetization of 63.034 emu/g. This technique can be a potential method to synthesize novel nickel ferrite nanostructure with improved magnetic properties [34].

In the work of V. Ratchagar et.al, the SnO_2 Nano materials were synthesized by chemical precipitate technique. The pH of the reaction solution was varied from 7 to 9 insteps of 1. From the powder XRD the particle size was calculated using Scherrer formula, it varied from 57 to 66 nm for different pH values. The FE-SEM analysis reveals the morphology of SnO2 nanomaterials. Vibrating sample magnetometer (VSM) results demonstrates that the SnO2 samples exhibit perfect room temperature ferromagnetism (RTFM). The sample was characterized by TGA/DTA. Measurement of different electrical parameters with frequency (50 Hz−5 MHz) has been carried out different temperature [35].

Another work done by P.M.Ponnusamya et.al Nano crystalline nickel oxide (NiO) and ferrous doped NiO dilute magnetic nanoparticles have been prepared by wet-chemical method. The structural, composition, morphology, UV absorption and magnetic analysis of the prepared samples are characterized by XRD, FESEM, HRTEM, UV Spectra and VSM. XRD confirms the FCC phase formation. The FESEM and HRTEM used to found the

structural parameters. The U–V absorption measurement shows the strong absorption at 313.24 nm and 307.9 nm for un doped NiO and Fe-doped NiO nanoparticles. The magnetic properties of these nanoparticles confirming the ferromagnetic behaviour at room temperature and has been attributed due to particle size effect [36].

Magnetic cores of passive components are required to have low hysteresis loss, which is dependent on the coercive force. Since it is well known that the coercive force becomes zero at the superparamagnetic regime below a certain critical size, Toshitaka Ishizaki et.al attempted to synthesize Ni nanoparticles in a size-controlled fashion and investigated the effect of particle size on the magnetic properties. Ni nanoparticles were synthesized by the reduction of Ni acetylacetonate in oleyl amine at 220 ◦C with strictly phosphine (TOP) as the capping agent. An increase in the TOP/Ni ratio resulted in the size decrease. We succeeded in synthesizing superparamagnetic Ni nanoparticles with almost zero coercive force at particle size below 20 nm by the TOP/Ni ratio of 0.8. However, the saturation magnetization values became smaller with decrease in the size. The saturation magnetizations of the Ni nanoparticles without capping layers were calculated based on the assumption that the interior atoms of the nanoparticles were magnetic, whereas the surface-oxidized atoms were non-magnetic. The measured and calculated saturation magnetization values decreased in approximately the same fashion as the TOP/Ni ratio increased, indicating that the decrease could be mainly attributed to increases in the amounts of capping layer and oxidized surface atoms [37].

Recently, iron oxide nanoparticles (NPs) have attracted much consideration due to their unique properties, such as superparamagnetic, surface-to-volume ratio, greater surface area, and easy separation methodology. Various physical, chemical, and biological methods have been adopted to synthesize magnetic NPs with suitable surface chemistry. The work done by Attarad Ali et.al summarizes the methods for the preparation of iron oxide NPs, size and morphology control, and magnetic properties with recent bioengineering, commercial, and industrial applications. Iron oxides exhibit great potential in the fields of life sciences such as biomedicine, agriculture, and environment. Nontoxic conduct and biocompatible applications of magnetic NPs can be enriched further by special surface coating with organic or inorganic molecules, including surfactants, drugs, proteins, starches, enzymes, antibodies, nucleotides, non-ionic detergents, and polyelectrolytes. Magnetic NPs can also be directed to an organ, tissue, or tumour using an external magnetic field for hyperthermia treatment of patients. Keeping in mind the current interest in iron NPs, this review is designed to report recent information from synthesis to characterization, and applications of iron NPs [38].

Nickel Oxide (NiO) is an important transition metal oxide with cubic lattice structure. Among the magnetic nanoparticles, fabrication of nickel nanoparticles is often more difficult than that of the other particles. This is because they are easily oxidized. To achieve pure nickel nanocrystals, numerous methods have been conducted in organic environments in order to prevent formation of hydroxide or oxidation. In the present work done by Fardin Taghizadeh, he reports the synthesis of NiO nanoparticles. Magnetic properties of NiO nanoparticles with different sizes and at different temperatures are compared. The phase structures, particle sizes and magnetic properties of NiO nanoparticles have been characterized by X-ray diffraction, TEM images and Vibrating Sample Magnetometer (VSM). The experimental data reported in the literature were collected, for the same conditions, and after fitting, extrapolating and doing some calculations. The magnetization for smaller nanoparticles is bigger for the samples we consider here. This difference could be explained by the difference of surface volume ratio of nanoparticle which shows the contribution of the paramagnetic surface is more important with respect to the anti-ferromagnetism of the core for smaller particles. Also the nanoparticle at lower temperatures shows bigger magnetization [39].

The influence of the particle size on magnetic behaviours of nickel oxide nanoparticles (NiO NPs) was reported by Tayebe Razegh et.al, NiO NPs with a uniform particle size were synthesized via a facile sol-gel method, and various sizes of NiO NPs (11, to 49 nm) were achieved by calcination at various temperatures (400, to 700 °C). X-ray diffraction (XRD) analysis revealed that increasing the calcination temperature increased the crystallite size. TEM observations and XRD analysis were used to determine the particle size of the NiO NPs. The field emission scanning electron microscopy (FESEM) and transmission electron microscopy (TEM) images showed flake-like morphologies, which consisted of interconnected nanoparticles with a porous channel. The magnetic properties of NiO NPs with different size were studied using vibrating sample magnetometer (VSM). The results suggested that the particle size plays an important role in magnetic property of NiO nanoparticles [40].

3.3 Nano Change of Electrical Properties

Many researches were done to study the effect of Nano structure on the electric properties. One of these attempts were made in the work of M.Dirar et.al [41] where show that doping polymer with Zno causes Fermi level to change with Zno concentration. Khadija also shows that doping polymer with Cuo also changes Fermi level due to the change of Cuo

concentration [42]. Thowra shows that changing the Zno and Cuo layer in FTO/Cuo/Zno/Al and FTO/Zno/Cuo/Al solar cell changes the electric power included [43].

3.4 Summary and Critique

Different attempts were made to show that changing Nano structure changes physical properties [44, 45, 46]. The optical properties can be changed [47, 48, 49] by changing Nano structure as well as the electric properties [50, 51, 52] and magnetic properties [53, 54, 55]. Even thermal properties can also be changed [56, 57, 58]. The change of these properties can be used in industry, medicine and all technology applications that are related to human needs [59, 60, 61]. Despite the intensive research made but still one needs more researches to development technology.

Chapter Four
Experimental Work

4.1 Materials

The materials that were used in the experiments are:-

Nickel oxide (Ni_2O_3):-

It that was prepared from nickel nitrate (Ni (NO_3)$_2$.$6H_2O$) (Hex hydrate) its colour is green. To prepare 0.1 M from nickel nitrate 6.6 g from nickel nitrate and solved it on 508 mL deionized water, and put the solution in the magnetic stirrer at 70^0C for 90 min and was added methanol to accelerate the reaction, after 90 min the colour of solution was changed from dark green to white green and one observe evaporate of hydrogen.

Iron oxide (Fe_3O_4):-

It can be prepared from Ferric nitrate (Fe (NO_3)$_3$.$9H_2O$) (Iron (III) nitrate) its colour was white, to prepare 0.1 M from Iron nitrate 40.4 g from iron nitrate that was solve it of 515 mL deionized water, and but the solution in the magnetic stirrer at 70^0C for 90 min and was added methanol to accelerate the reaction, after 90 min the colour of solution was change from white yellow to brown and we were observe evaporate of hydrogen gas that was observe it from smile.

4.2 Tools and instruments

The tools that were used in the experiment to study the materials optical and magnetic properties are:-

4.2.1 X-Ray Diffract meter (XRD)

The crystal structure of all samples was characterized at room temperature using a Philips PW1700 X-ray diffract meter (operated at 40 kV and current of 30 mA) and samples were scanned between 200 and 900 at a scanning speed of 0.06 ^{o}C/s using Cu Kα radiation with λ = 1.5418Å.

4.2.2 UV-VIS Spectrophotometer

The optical measurements comprise measuring the absorbance and transmittance is within the range of (350 - 900 nm), in the current study, one use (UV-1650PC Shimadzu software 1700, 1650, UV-visible recording spectrophotometer).

4.2.3 Scanning Electron Microscope (SEM)

(SEM, Tuscan Vega LMU).

4.3 Method

The method that was used in the experiment was:-

4.3.1 Experimental Procedure of Ni_2O_3 and Fe_3O_4 Preparation

Nickel oxide thin films were prepared by spraying a 0.1 M solution of nickel nitrate of doubly distilled water onto the pre-heated amorphous glass substrates kept at 390˚C ± 10˚C. While iron oxide thin films were prepared by spraying a 0.1 M solution of ferric nitrate of doubly distilled water onto the pre-heated amorphous glass substrates kept at 390˚C ± 10˚C. Film thickness was measured by using the weight difference method considering the density of the bulk nickel oxide. As the density of thin films was certainly lower than the bulk density, the actual film thickness would be larger than the estimated values. The structural, optical characterization of the films deposited at optimized preoperative parameters was carried out. The optical measurements comprise measuring the absorbance and transmittance with range (350 - 900 nm), in the current study, by using (UV-1650PC Shimadzu software 1700, 1650, UV-visible recording spectrophotometer). The thickness is an effective method for estimating the type of charge carrier (n-type or p-type) especially those materials of large energy gap and transport mechanism in polycrystalline semiconductors.

4.3.2 Thin film preparation

The spray pyrolysis method used here is basically a chemical deposition method in which fine droplets of the desired material are sprayed onto a heated substrate. Continuous films are formed on the hot substrate by thermal decomposition of the material droplets.

The Fe_3O_4 films were deposited onto glass slides, chemically cleaned, using the spray pyrolysis method at 170^0 C substrate temperature. Concentration of 0.2 mM of (NH O_3 Fe) in solvent was used for all the films. The nozzle to substrate distance was 30 cm and during deposition, solution flow rate was held constant at 2 ml/min. The substrate temperature was measured using an Iron-Constantan thermocouple. The thickness of the thin films was measured by weight difference method using a sensitive microbalance.

The optical measurements of Fe_3O_4 film were carried out at room temperature using UV Spectrophotometer in the wavelength range from 287 to 447 nm. The substrate absorption is corrected by introducing an uncoated cleaned glass substrate in the reference beam.

4.3.3 Spin coating method

Spin coating is a procedure used to deposit uniform thin films to flat substrates. Usually a small amount of coating material is applied on the centre of the substrate, which is either

spinning at low speed or not spinning at all. The substrate is then rotated at high speed in order to spread the coating material by centrifugal force. A machine used for spin coating is called a spin coater, or simply spinner.

Rotation is continued while the fluid spins off the edges of the substrate, until the desired thickness of the film is achieved. The applied solvent is usually volatile, and simultaneously evaporates. The higher the angular speed of spinning, the thinner the film. The thickness of the film also depends on the viscosity and concentration of the solution, and the solvent [62].

The pioneering theoretical analysis of spin coating was undertaken by Emslie et al [63], and has been extended by many subsequent authors (including Wilson et al [64], who studied the rate of spreading in spin coating).

Spin coating is widely used in micro fabrication of functional oxide layers on glass or single crystal substrates using sol-gel precursors, where it can be used to create uniform thin films with nanoscale thicknesses [65]. It is used intensively in photolithography, to deposit layers of photoresist about 1 micrometre thick. Photoresist is typically spun at 20 to 80 revolutions per second for 30 to 60 seconds.

This process has been widely used in the manufacture of integrated circuits, optical mirrors, colour television screens and magnetic disk for data storage. Centrifugal force drives the liquid radial outward. The viscous force and surface tension causes a thin residual film to be retained on the flat substrate. The film thins by the combination of outward fluid flow and evaporation [66].

4.3.4 ITO Glass

Conductive thin films have various applications in different technological fields. Indium tin oxide (ITO) is a mixed oxide. In the film form, ITO has been widely employed as electrode in many optoelectronic devices. Methods like thermal evaporation, sputtering, chemical vapour deposition (CVD), electron beam, spray coating, and sol-gel synthesis give ITO thin films. ITO consisted of spherical particles with different diameters. The ITO thin films were treated with laser. X-ray diffraction (XRD) analysis confirmed that spray pyrolysis produced spherical ITO particles. Transmittance analyses revealed the production of transparent films with thicknesses ranging from 0.800 to 1.200 μm. The four-wire test showed that the porosity of the films led to low conductivity. Film resistance is a function of the number of layers of ITO thin film [67].

Chapter Five

Results, Discussion, Conclusion and Recommendation

5.1 Introduction

In this research five Fe_3O_4 and five Ni_2O_3 samples were deposited on ITO substrate by changing their concentration. The change of absorption coefficient, energy gap, magnetic permeability and electric permittivity with concentrations and Nano size was studied here. The results obtained, beside discussion and conclusion were exhibited in this chapter.

5.2 Results

5.2.1.1 Ni₂O₃ (Nickel Oxide) XRD, Magnetic and Electric Results

From figure it clear that the relationship between intensity and angle
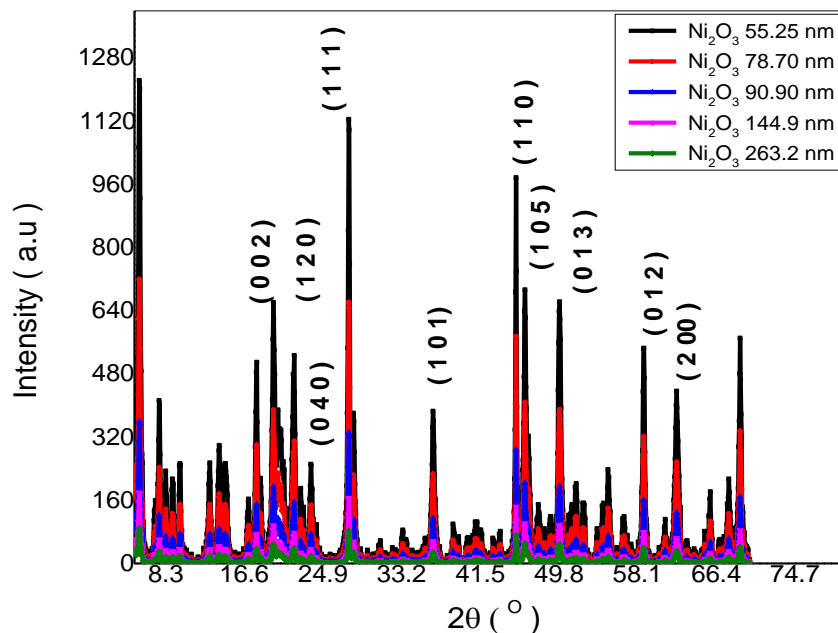
Fig(5.1) the XRD charts of the five Ni₂O₃ (Nickel Oxide) sample

The table explains some crystallite lattice parameter:-

Table (5.1) some crystallite lattice parameter (c- form , a,b,c, β,α, γ, density ,Xs(nm) and d – spacing) of all samples that meade by five Ni_2O_3 (Nickel Oxide) sample

Sample	C-form	a	b	c	α	β	γ	Density(g.cm⁻³)	Xs(nm)	d-spacing (Aº)
Ni_2O_3: 55.25 nm	Hexagonal/Primitivty	4.61	4.61	5.61	90	90	120	5.3175	53	2.74230
Ni_2O_3: 78.7 nm	Hexagonal/Primitivty	4.61	4.61	5.61	90	90	120	5.3175	55.75	4.07930
Ni_2O_3: 90.9 nm	Hexagonal/Primitivty	4.523	4.523	7.36	90	90	120	5.434	56.15	4.07975
Ni_2O_3: 144.9 nm	Hexagonal/Primitivty	2.955	2.955	7.227	90	90	120	6.803	57.03	4.08000
Ni_2O_3: 263.2 nm	Hexagonal/Primitivty	2.818	2.818	20.56	90	90	120	7.435	57.44	9.02055

The table explains the relationship between concentration and Electrical permittivity (ε) and magnetic permeability (µ):-

Table (5.2) Electrical permittivity (ε) and magnetic permeability (µ) for all five Ni_2O_3 samples

Concentration (mg/cm²)	Electrical permittivity/ε (farad/nm)	Magnetic permeability/µ $\times 10^{-18}$ (hennery/nm)
263.15	0.26555	11.0822
144.9	0.21389	9.50604
90.9	0.14952	6.64518
78.7	0.12569	5.58615
55.25	0.07746	3.4426

The Figurues explain the relationship between thicknesses and density and crystal size
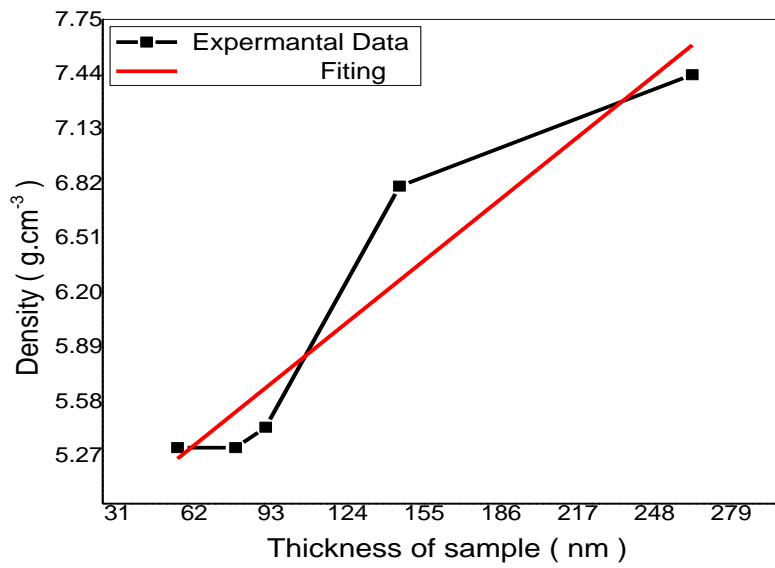
Fig(5.2) Dependence of the density on the five Ni$_2$O$_3$ (Nickel Oxide) sample
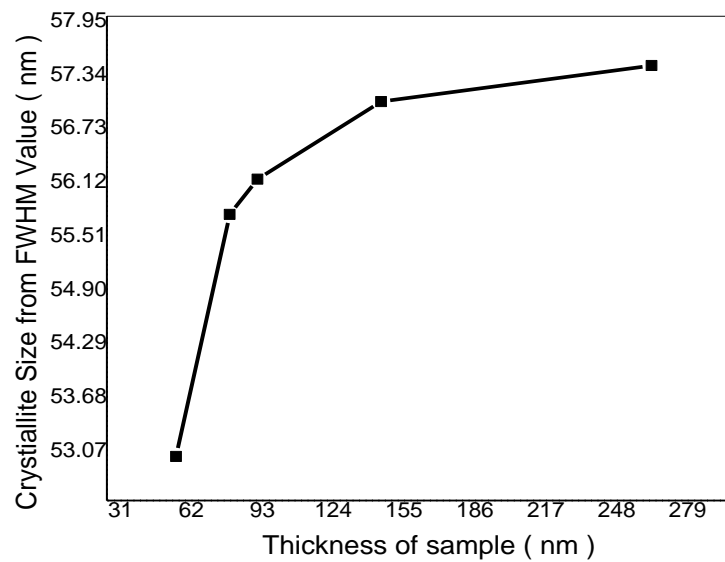
Fig (5.3) Dependence of the crystallites growth on the five Ni$_2$O$_3$ (Nickel Oxide) sample

The Figurues explain the relationship between thicknesses and d-spacing and permitivity
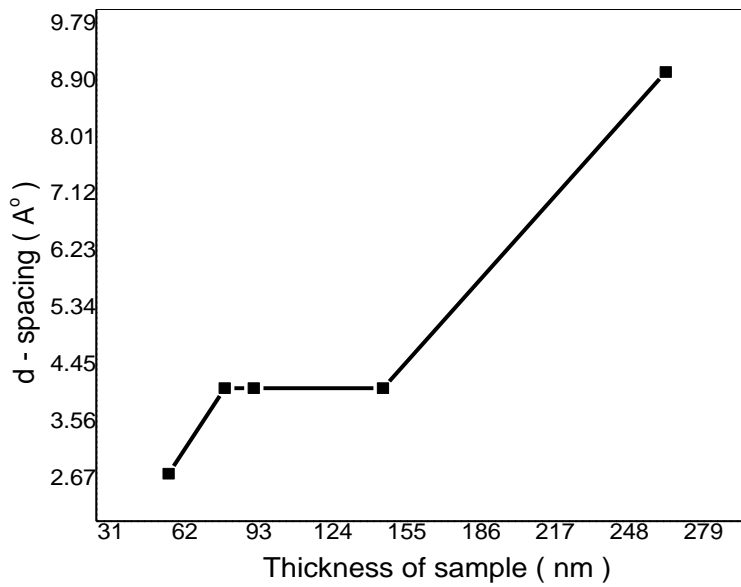
Fig(5.4) Dependence of the d- spacing on the five Ni$_2$O$_3$ (Nickel Oxide) sample
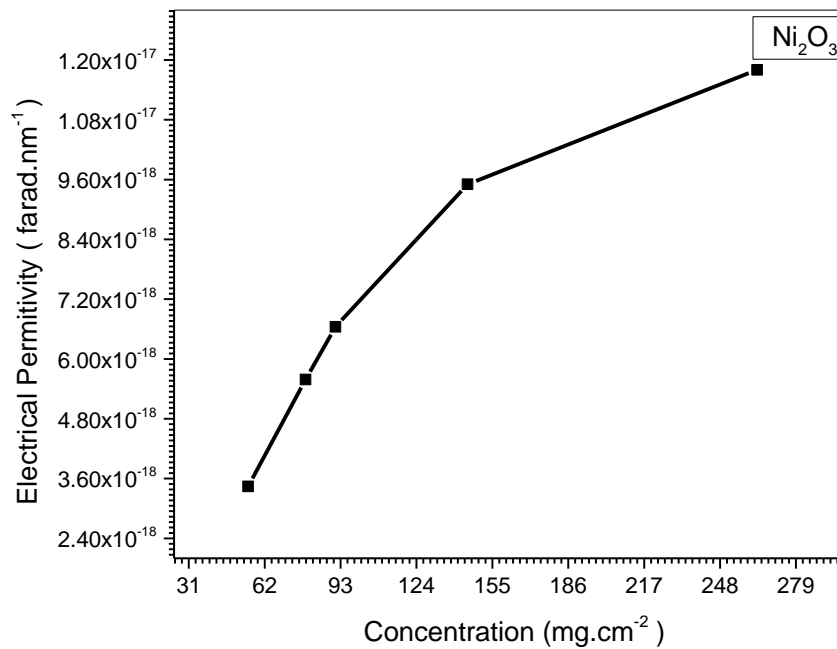
Fig(5.5) relationship between electrical permittivity and concentration of the five Ni$_2$O$_3$ (Nickel Oxide) sample

The Figurues explain the relationship between concentration and magnetic permeability
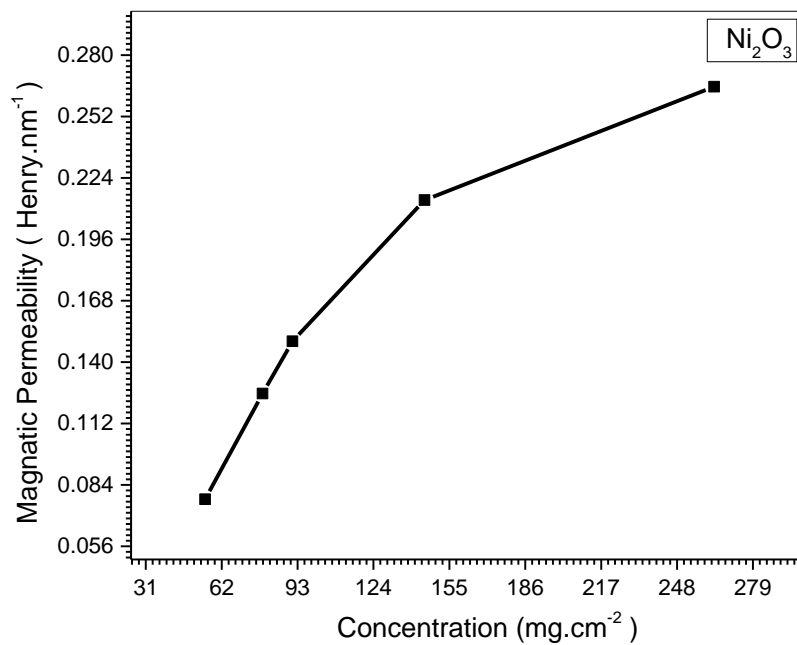
Fig(5.6) releationship between magnetic permeability and concentration of the five Ni₂O₃ (Nickel Oxide) sample

5.2.1.2 Fe₃O₄ (Iron Oxide) XRD, Magnetic and Electric Results

5.2.1.2 Fe$_3$O$_4$ (Iron Oxide)   XRD, Magnetic and Electric Results

From figure it clear that the relationship between intensity and angle
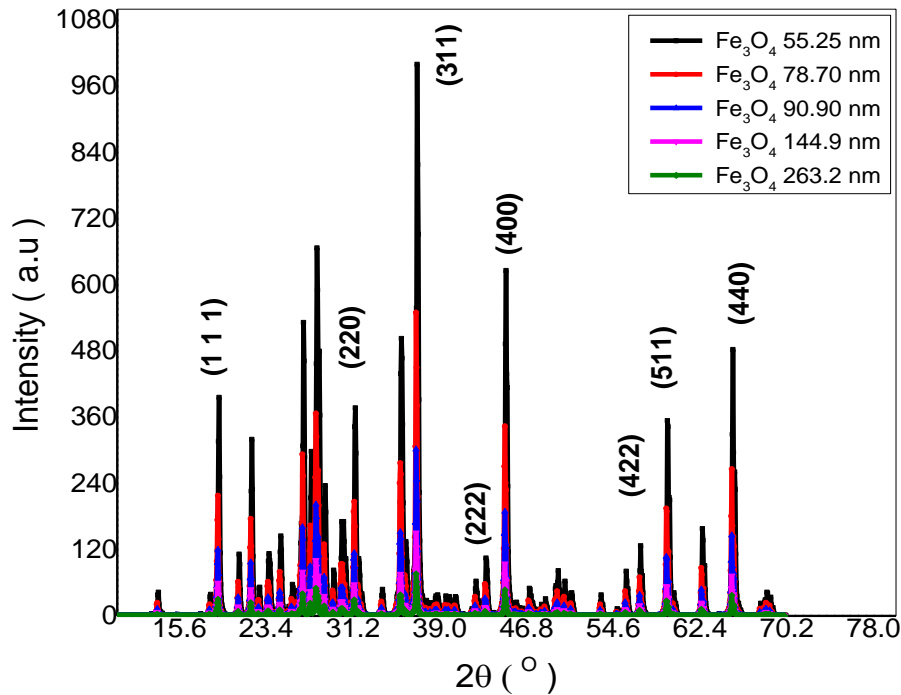
Fig(5.7) the XRD charts of the five Fe$_3$O$_4$ (Iron Oxide) sample

The table explains some crystallite lattice parameter:-

Table (5.3) some crystallite lattice parameter (c- form , a,b,c, β,α, γ, density ,Xs(nm) and d – spacing) of all samples that made by five Fe$_2$O$_3$ (Iron Oxide) sample

Sample	C-form	a	b	c	α	β	γ	Density(g.cm^{-3})	Xs(nm)	d-spacing (A^o)
Fe$_3$O$_4$: 55.25 nm	Cubic /F-Center	8.09	8.09	8.09	90	90	90	4.857	55.05	3.0297
Fe$_3$O$_4$: 78.7 nm	Cubic /F-Center	8.39	8.39	8.39	90	90	90	5.102	56.06	2.21935
Fe$_3$O$_4$: 90.9 nm	Cubic /F-Center	8.39	8.39	8.39	90	90	90	5.2071	56.10	2.22425
Fe$_3$O$_4$: 144.9 nm	Cubic /Primitivty	8.35	8.35	8.35	90	90	90	5.2071	62.95	2.6007
Fe$_3$O$_4$: 263.2 nm	Cubic /I-Center	9.4	9.4	9.4	90	90	90	5.808	64.25	3.59315

The table explains the relationship between concentration and Electrical permittivity (ε) and magnetic permeability (µ):-

Table (5.4) Electrical permittivity (ε) and magnetic permeability (µ) for all five Fe₃O₄ samples

Concentration (mg/cm^2)	Electrical permittivity/ε (farad/nm)	Magnetic permeability/µ $\times 10^{-17}$ (hennery/nm)
263.15	0.44343	1.97079
144.9	0.47716	2.12073
90.9	0.49507	2.20031
78.7	0.52125	2.31665
55.25	0.52457	2.3314

The Figurue explain the relationship between thickness and density
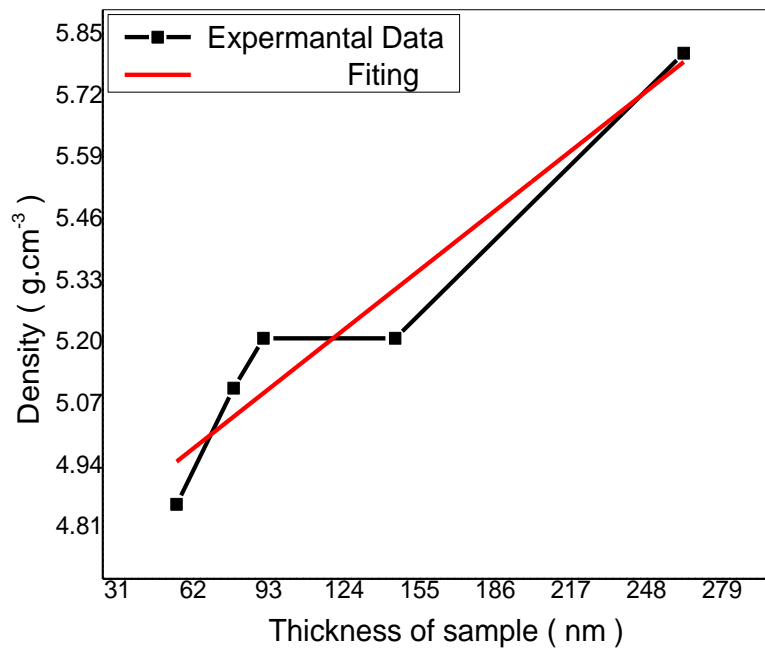
Fig(5.8) Dependence of the density on the five Fe₃O₄ (Iron Oxide) sample

The Figurues explain the relationship between thickness and crystal size, d-spacing
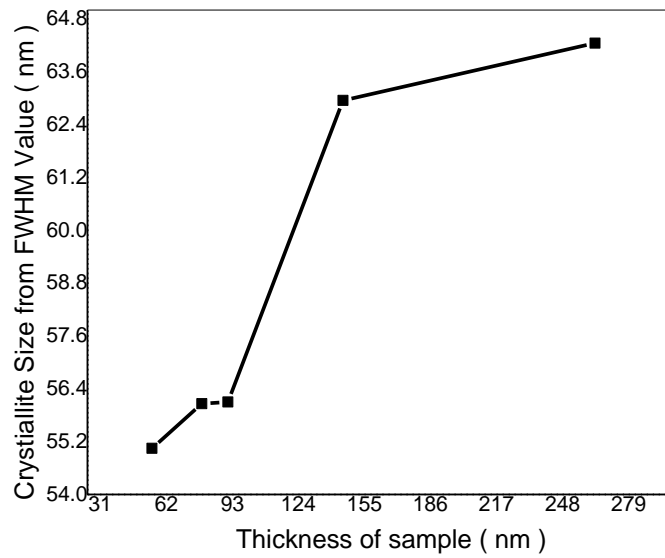
Fig (5.9) Dependence of the crystallites growth on the five Fe$_3$O$_4$ (Iron Oxide) sample
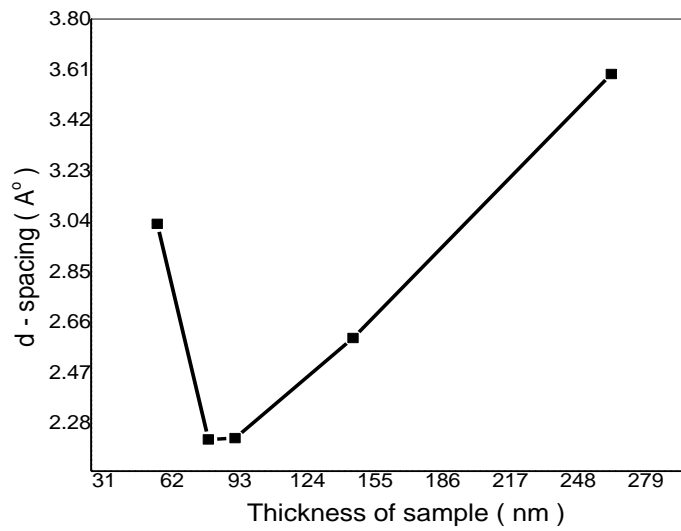
Fig(5.10) Dependence of the d- spacing on the five Fe$_3$O$_4$ (Iron Oxide) sample

The Figurues explain the relationship between concentration and permeabilit, permitivity
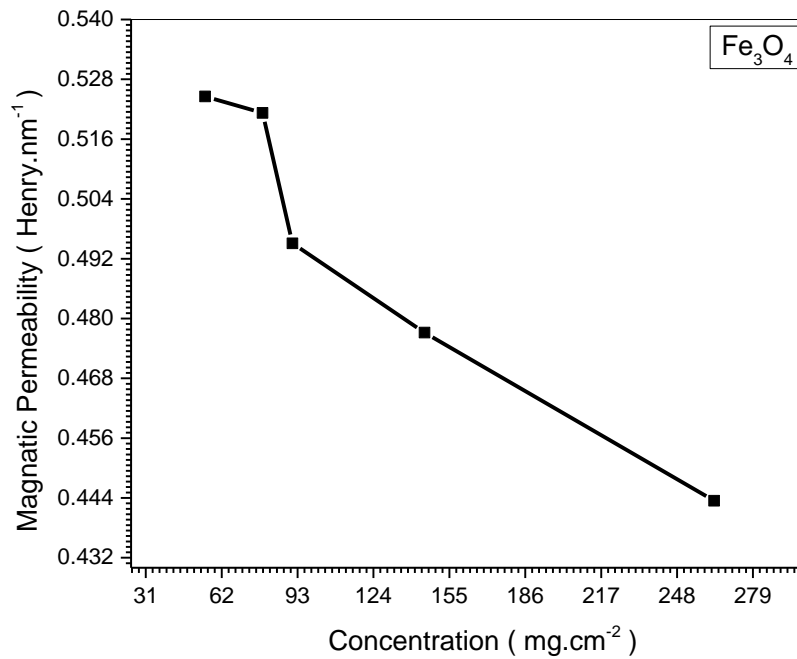
Fig(5.11) relationship between magnetic permeability and concentration of the five Fe₃O₄ (Iron Oxide) sample
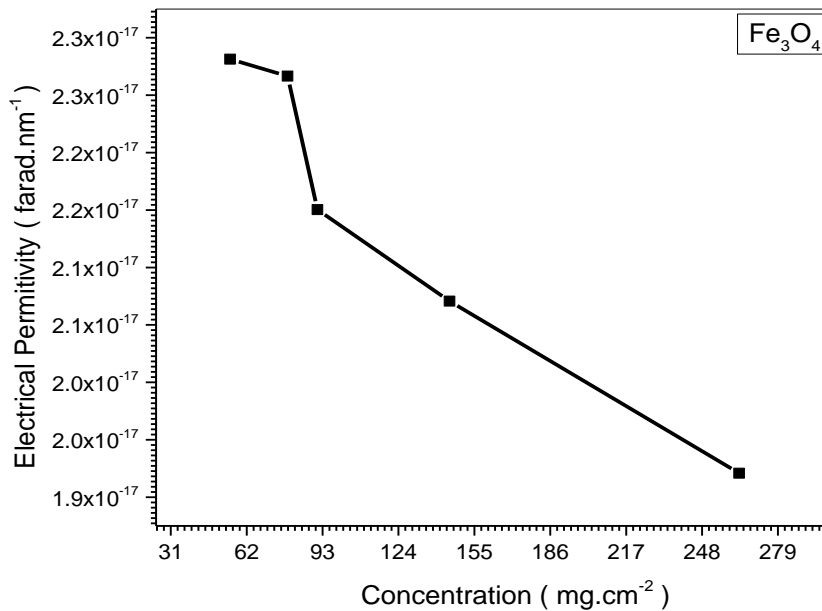
Fig(5.12) relationship between electrical permittivity and concentration of the five Fe₃O₄ (Iron Oxide) sample

5.2.2 SEM Results

5.2.2.1 Ni$_2$O$_3$ SEM Results

The Figurues explain the SEM images and Particle diameter distribution for
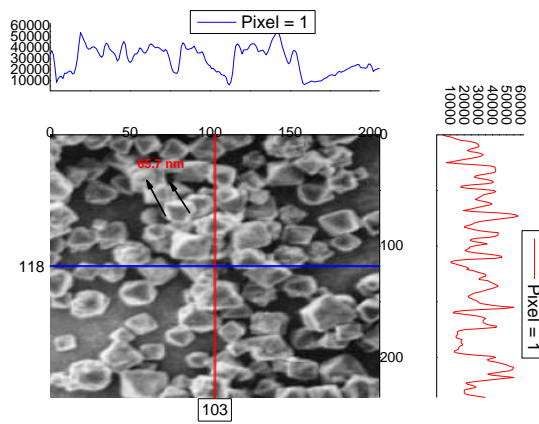
(Ni$_2$O$_3$: 55.25 nm)
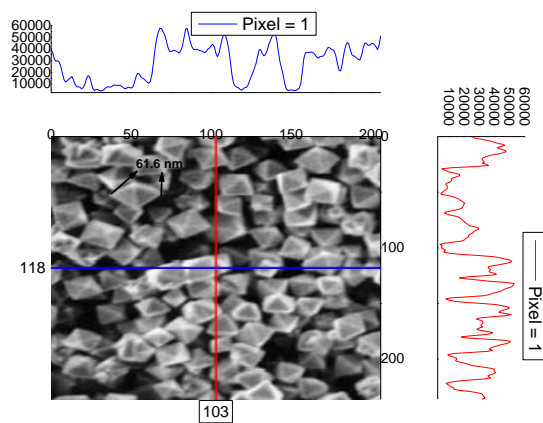
Fig (5.13) SEM images of the Ni$_2$O$_3$ sample films were thickness is 55.25 nm

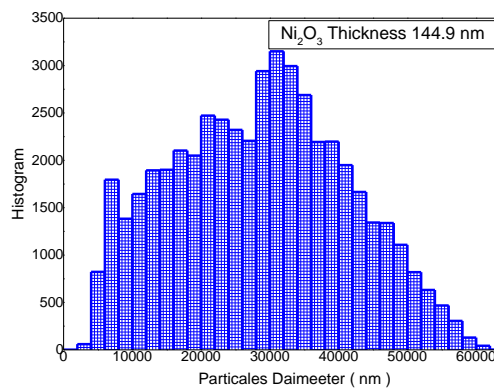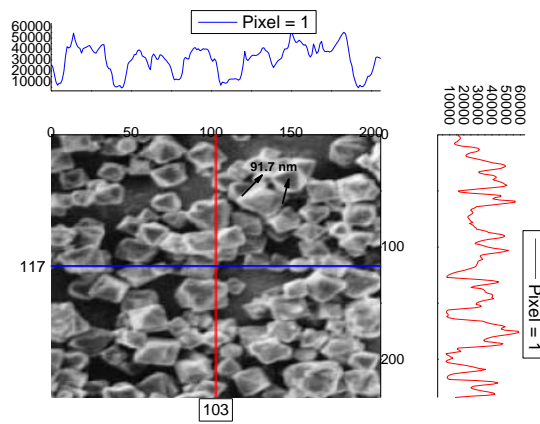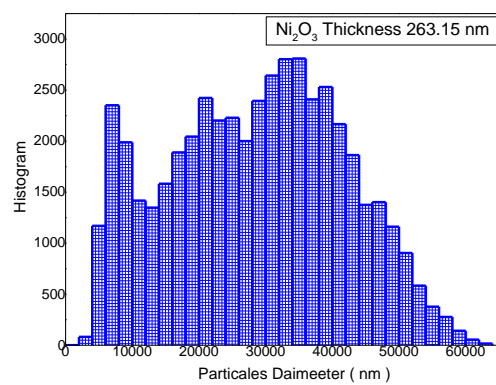**(The average size is 61.6 nm)**
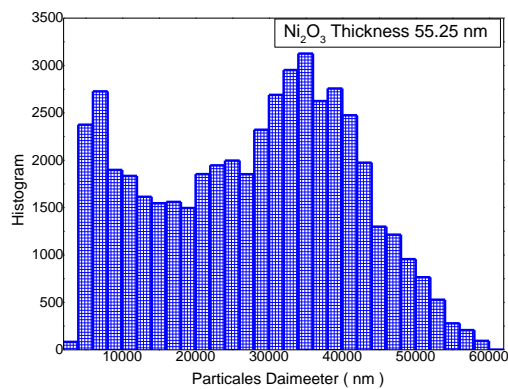
Fig (5.14) Particle diameter distribution of Ni$_2$O$_3$ sample films were thickness is 55.25

nm

The Figurues explain the SEM images and Particle diameter distribution for

(Ni_2O_3: 78.7 nm)
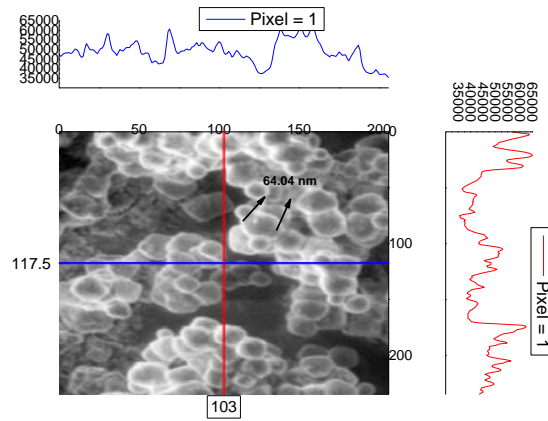
Fig (5.15) SEM images of the Ni_2O_3 sample films were thickness is 78.7 nm

(The average size is 64.04 nm)
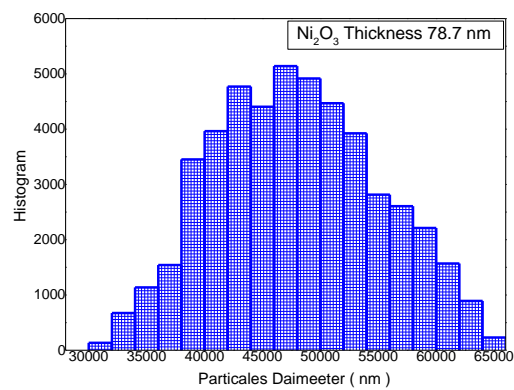
Fig (5.16) Particle diameter distribution of Ni_2O_3 sample films were thickness is 78.7 nm

The Figurues explain the SEM images and Particle diameter distribution for

(Ni_2O_3: 90.9 nm)
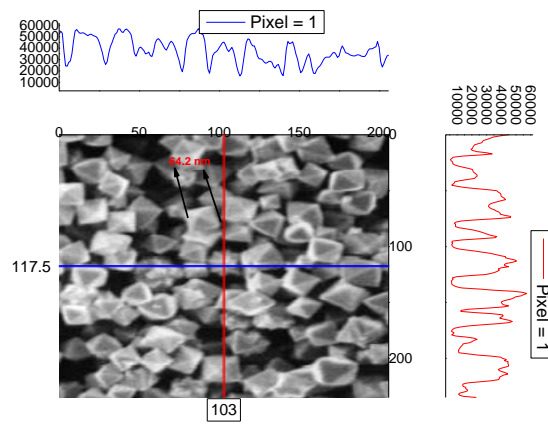
Fig (5.17) SEM images of the Ni_2O_3 sample films were thickness is 90.9 nm

(The average size is 64.2 nm)
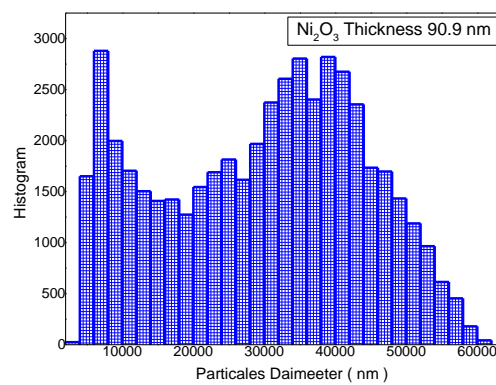
Fig (5.18) Particle diameter distribution of Ni_2O_3 sample films were thickness is 90.9 nm

The Figurues explain the SEM images and Particle diameter distribution for

(Ni_2O_3: 144.9 nm)

Fig (5.19) SEM images of the Ni_2O_3 sample films were thickness is 144.9 nm

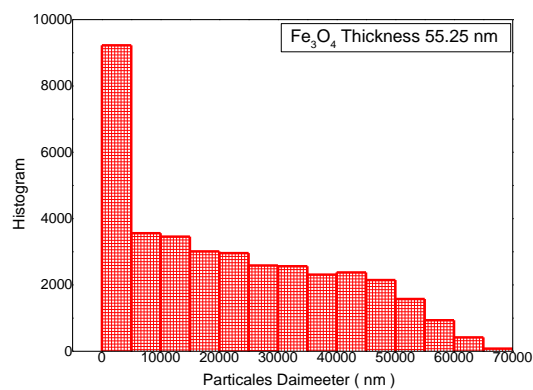**(The average size is 65.7 nm)**

Fig (5.20) Particle diameter distribution of Ni_2O_3 sample films were thickness is 144.9 nm

The Figurues explain the SEM images and Particle diameter distribution for

(Ni$_2$O$_3$: 263.15 nm)

Fig (5.21) SEM images of the Ni$_2$O$_3$ sample films were thickness is 263.15 nm

(The average size is 91.7 nm)

Fig (5.22) Particle diameter distribution of Ni$_2$O$_3$ sample films were thickness is 263.15 nm

5.2.2.2 Fe₃O₄ SEM Results

The Figurues explain the SEM images and Particle diameter distribution for

(Fe$_3$O$_4$: 55.25 nm)
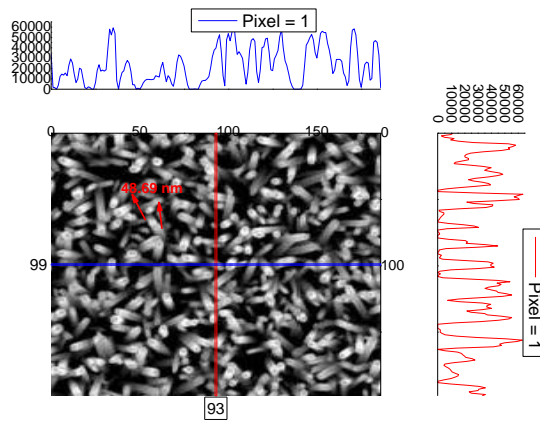
Fig (5.23) SEM images of the Fe$_3$O$_4$ sample films were thickness is 55.25 nm
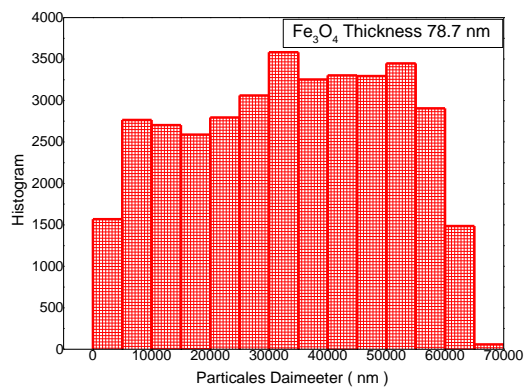
(The average size is 48.69 nm)

Fig (5.24) Particle diameter distribution of Fe$_3$O$_4$ sample films were thickness is 55.25 nm

The Figurues explain the SEM images and Particle diameter distribution for

(Fe$_3$O$_4$: 78.7 nm)
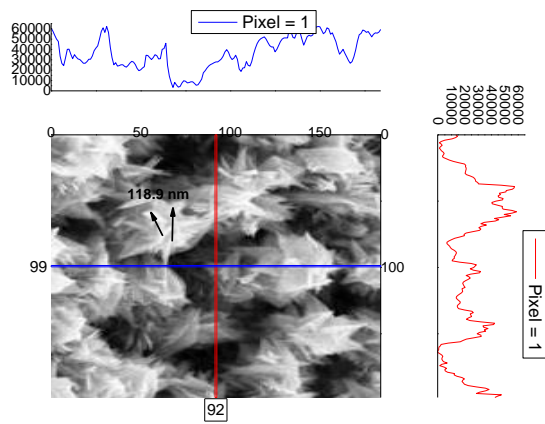
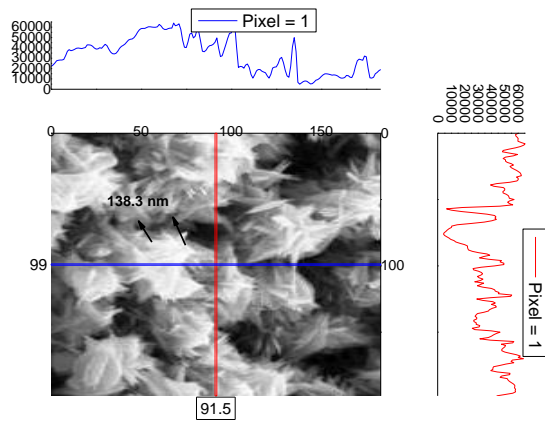**Fig (5.25) SEM images of the Fe $_3$O$_4$ sample films were thickness is 78.7 nm**
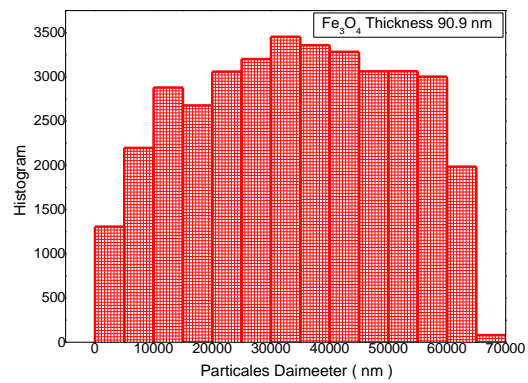
(The average size is 118.9 nm)

Fig (5.26) Particle diameter distribution of Fe$_3$O$_4$ sample films were thickness is 78.7 nm

The Figurues explain the SEM images and Particle diameter distribution for

(Fe₃O₄: 90.9 nm)

Fig (5.27) SEM images of the Fe₃O₄ sample films were thickness is 90.9 nm

(The average size is 138.3 nm

Fig (5.28) Particle diameter distribution of Fe₃O₄ sample films were thickness is 90.9 nm

The Figurues explain the SEM images and Particle diameter distribution for
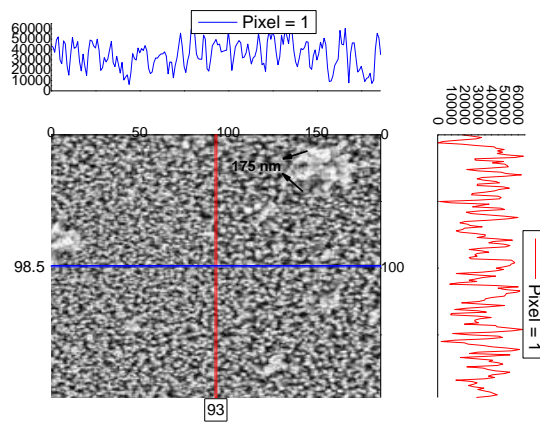
(Fe_3O_4: 144.9 nm)

Fig (5.29) SEM images of the Fe_3O_4 sample films were thickness is 144.9 nm

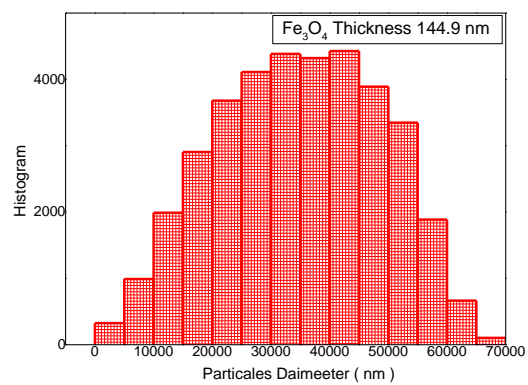**(The average size is 175 nm)**

Fig (5.30) Particle diameter distribution of Fe_3O_4 sample films were thickness is144.9 nm

The Figurues explain the SEM images and Particle diameter distribution for

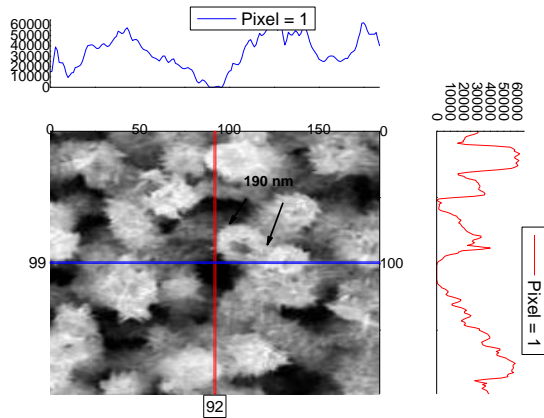**(Fe$_3$O$_4$: 263.15 nm)**

Fig (5.31) SEM images of the Fe$_3$O$_4$ sample films were thickness is 263.15 nm
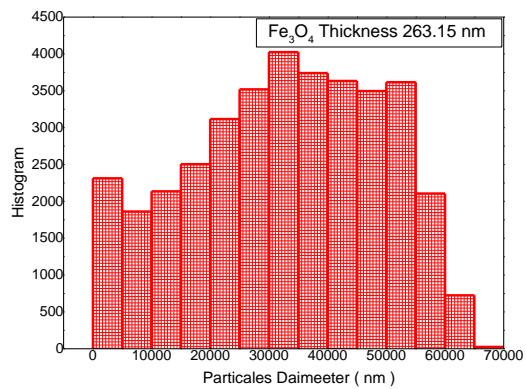
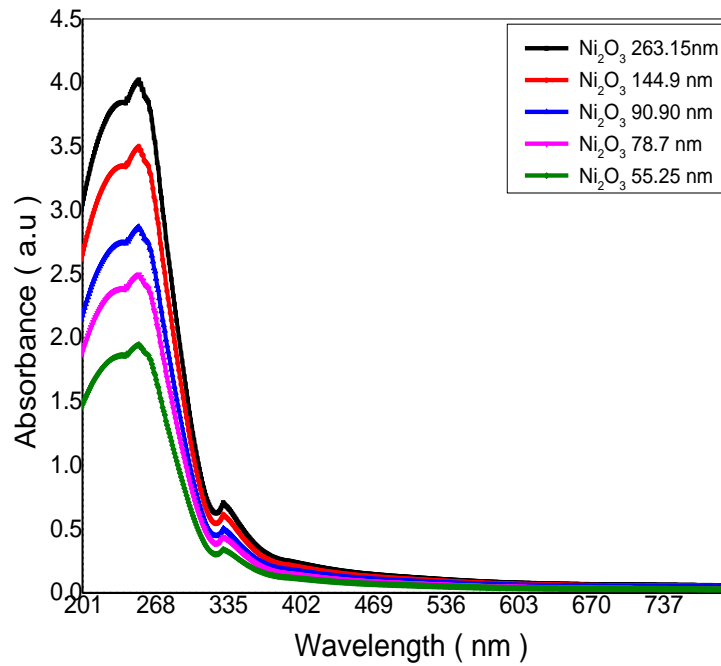**(The average size is 190 nm)**

Fig (5.32) Particle diameter distribution of Fe$_3$O$_4$ sample films were thickness is 263.15
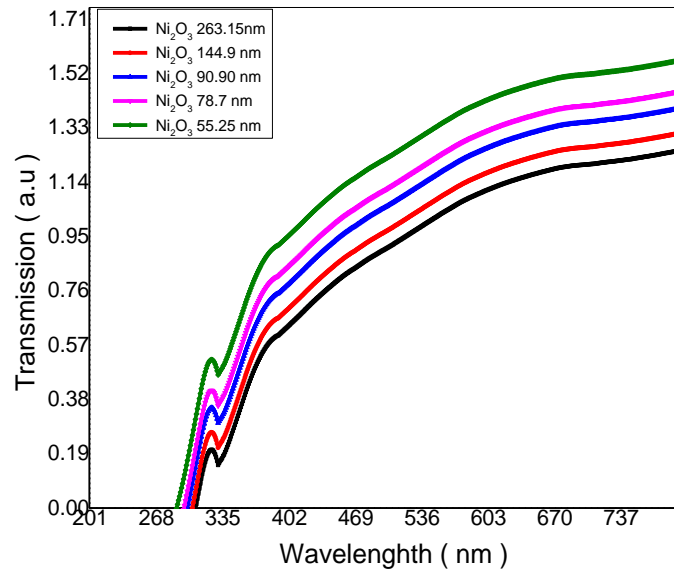
nm

5.2.3 Optical Results

5.2.3.1 Ni_2O_3 Optical   Results

The figure explain the relationship between absorbance and wavelengths

Fig(5.33) relation between absorbance and wavelengths of five sample that made by Ni_2O_3 in different thickness

The figure explain the relationship between wavelength and transmission, reflection

Fig(5.34) relation between transmission and wavelengths of five sample that made by Ni₂O₃ in different thickness
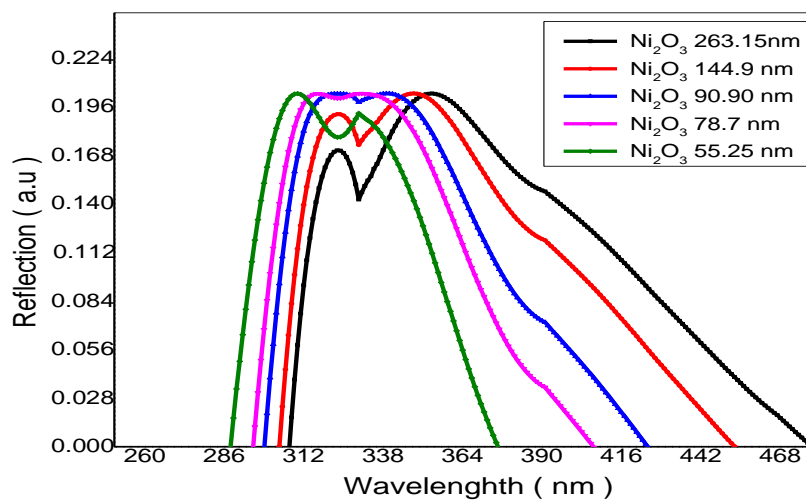

Fig(5.35) relation between reflection and wavelengths of five sample that made by Ni₂O₃ in different thickness

The figure explain the relationship between wavelength and absorption, extinction coefficient

Fig(5.36) relation between absorption coefficient and wavelengths of five sample that made by Ni$_2$O$_3$ in different thickness
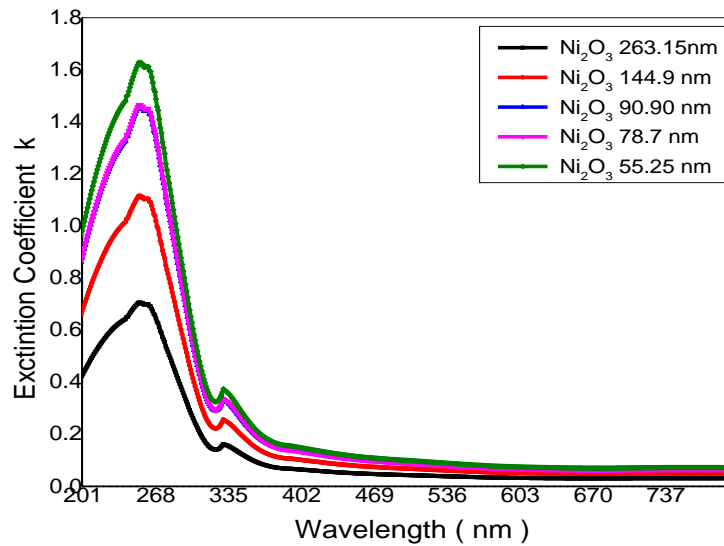
Fig(5.37) relation between extinction coefficient and wavelengths of five sample that made by Ni$_2$O$_3$ in different thickness

61

The figure explain the relationship between wavelength and refractive index, energy gap
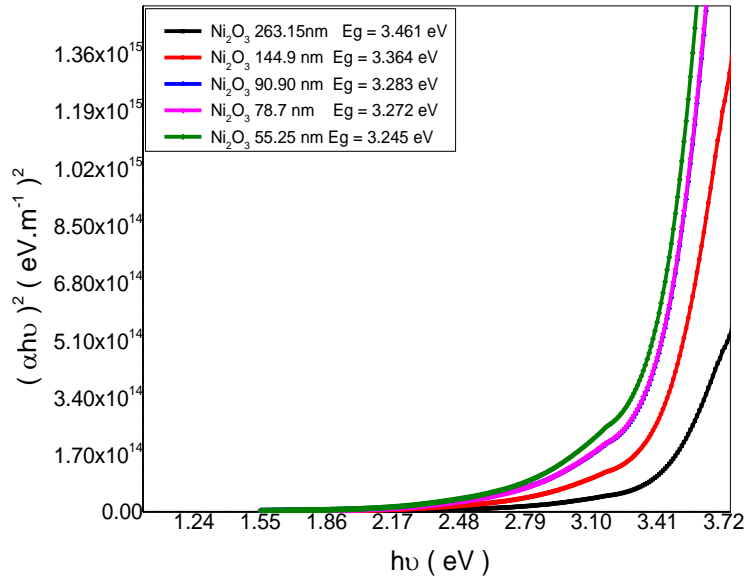
Fig(5.38)The optical energy band gap of five sample that made by Ni$_2$O$_3$ in different thickness
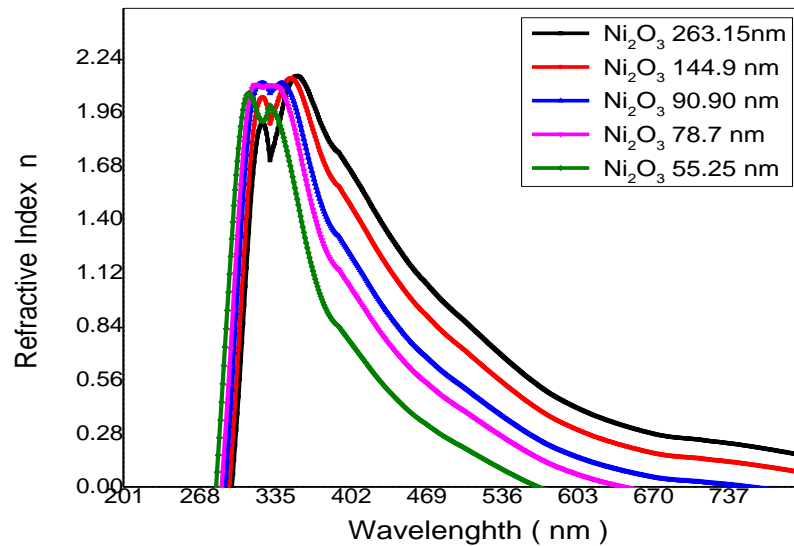
Fig(5.39) relation refractive index and wavelengths of five sample that made by Ni$_2$O$_3$ in different thickness

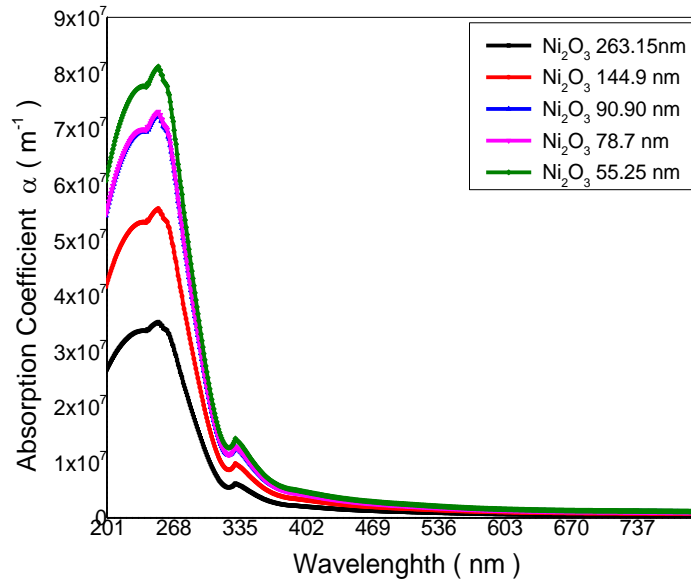**The figure explain the relationship between wavelength and real, imaginary dielectric constant**
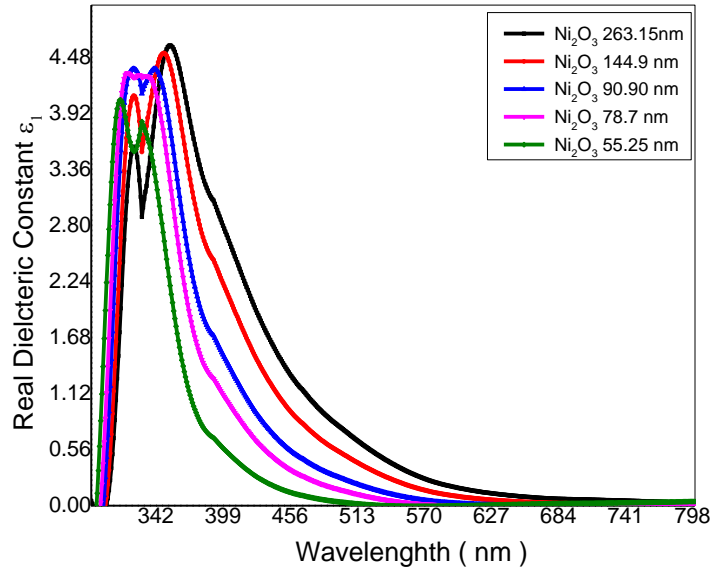
Fig (5.40) The relation between real dielectric constant and wavelengths of five sample that made by Ni$_2$O$_3$ in different thickness

Fig(5.41) The relation between imaginary dielectric constant and wavelengths of five sample that made by Ni$_2$O$_3$ in different thickness

The figure explain the relationship between wavelength and optical, electric conductivity

Fig (5.42) The relation between optical conductivity and wavelengths of five sample that made by Ni₂O₃ in different thickness

Fig (5.43) The relation between electrical conductivity and wavelengths of five sample that made by Ni₂O₃ in different thickness

5.2.3.1 Fe_3O_4 Optical Results

The figure explain the relationship between wavelengths and absorbance
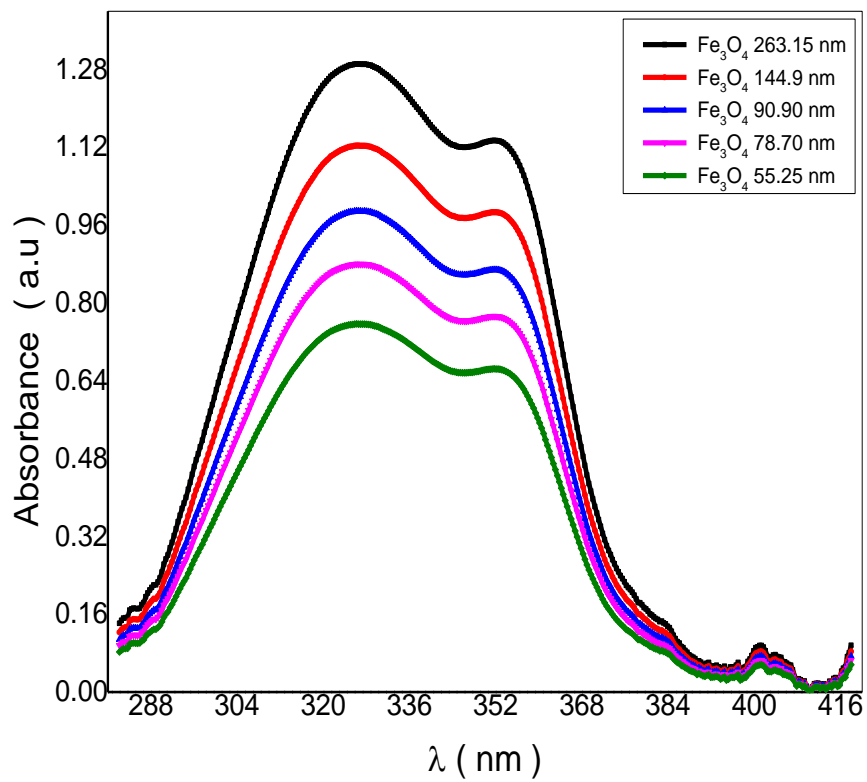
Fig(5.44) relation between absorbance and wavelengths of five sample that made by Fe_3O_4 in different thickness

The figure explain the relationship between wavelengths and transmission, raflection
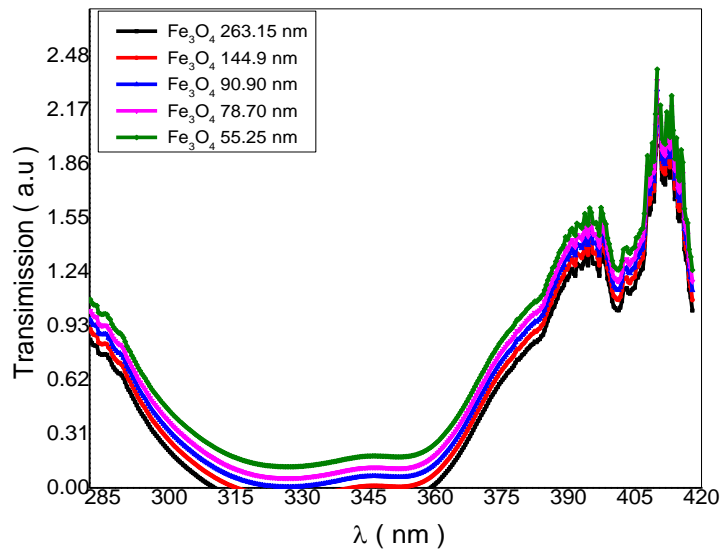
Fig(5.45) relation between transmission and wavelengths of five sample that made by Fe₃O₄ in different thickness
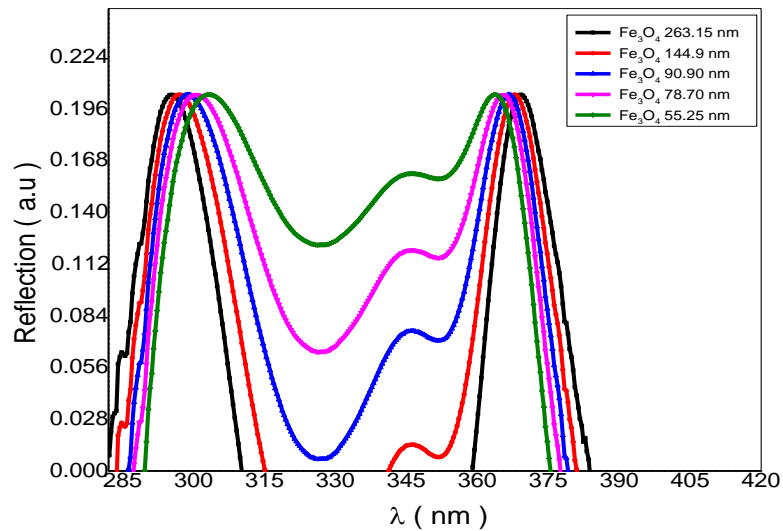
Fig(5.46)relation between reflection and wavelengths of five sample that made by Fe₃O₄ in different thickness

The figure explain the relationship between wavelengths and absorption, exctintion coefficient
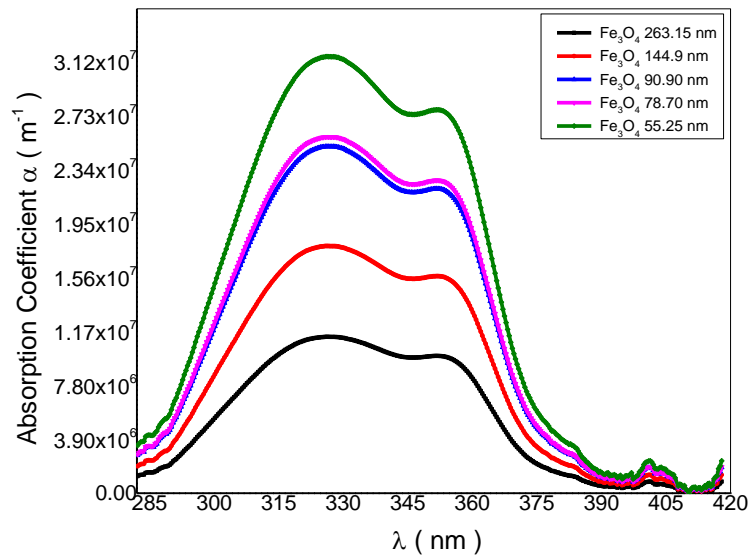
Fig(5.47) relation between absorption coefficient and wavelengths of five sample that made by Fe_3O_4 in different thickness
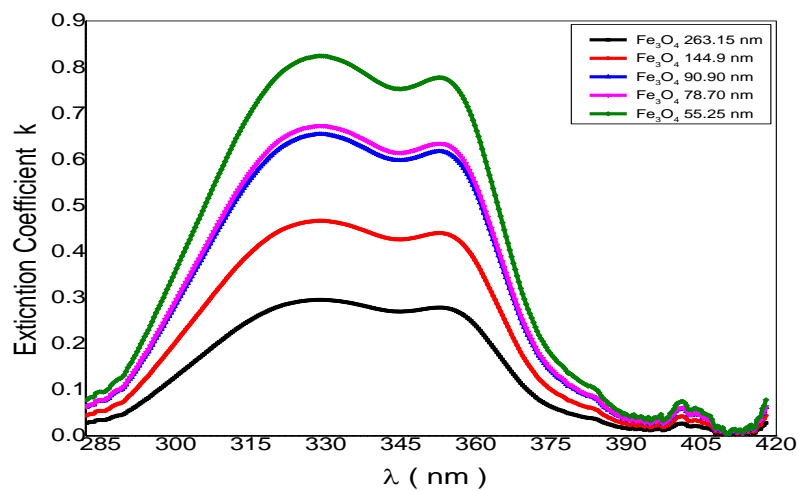
Fig(5.48) relation between exction coefficient and wavelengths of five sample that made by Fe_3O_4 in different thickness

The figure explain the relationship between wavelengths and energy gab, refractive index
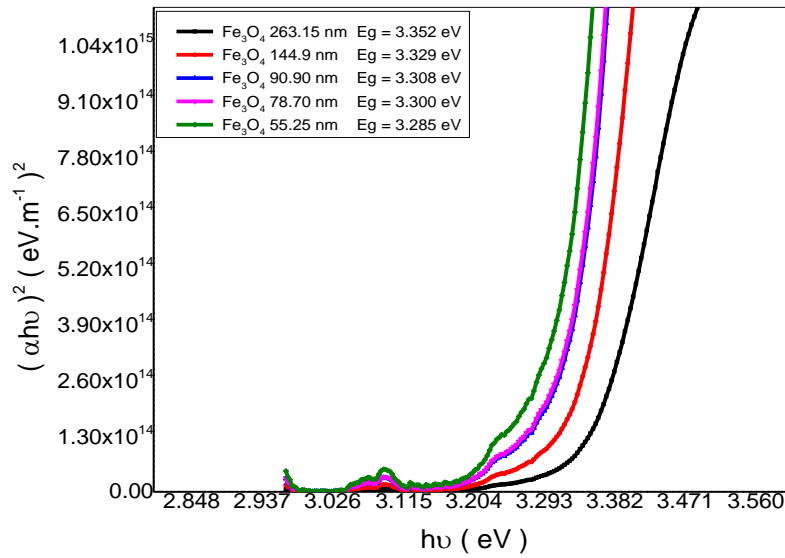
Fig(5.49)The optical energy band gap of five sample that made by Fe$_3$O$_4$ in different thickness
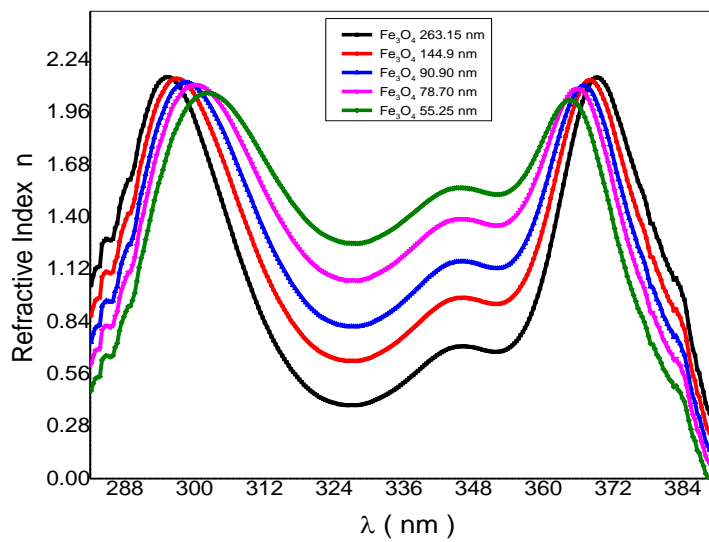
Fig(5.50) relation refractive index and wavelengths of five sample that made by Fe$_3$O$_4$ in different thickness

The figure explain the relationship between wavelengths and real, imaginary dielectric constant
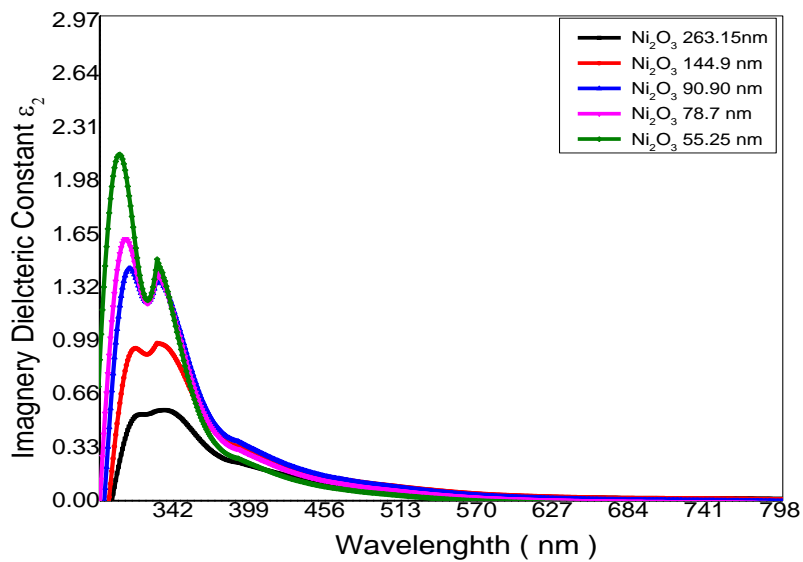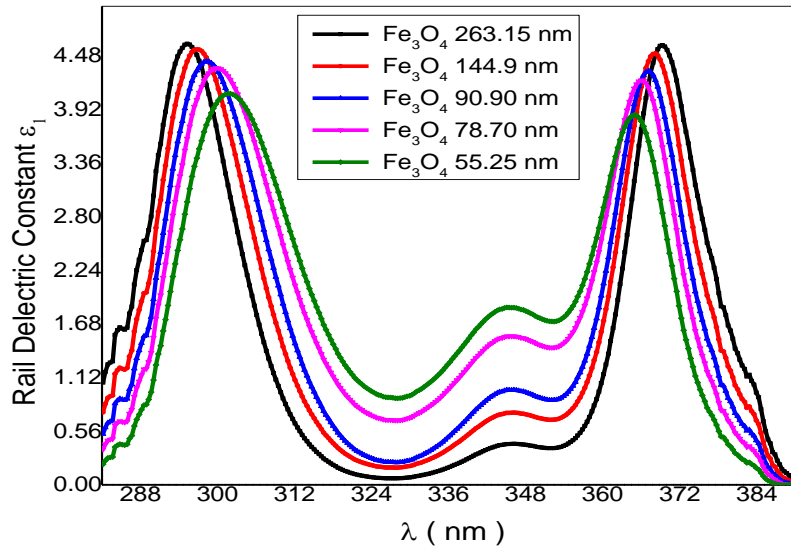

Fig (5.51)The relation between real dielectric constant and wavelengths of five sample that made by Fe₃O₄ in different thickness
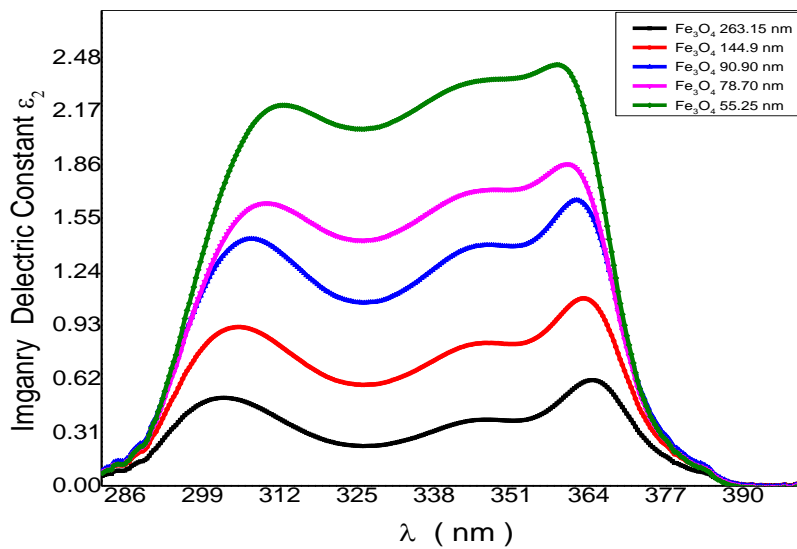
Fig (5.52)The relation between imagniary dielectric constant and wavelengths of five sample that made by Fe₃O₄ in different thickness

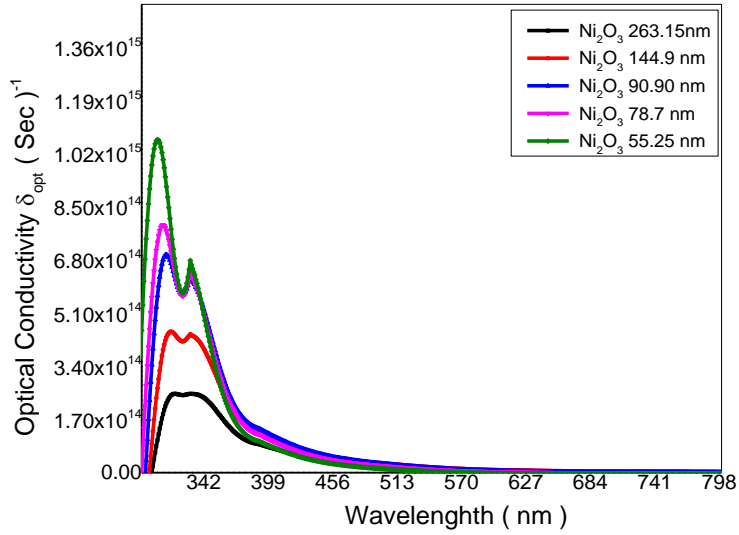**The figure explain the relationship between wavelengths and optical, electric conductivity**
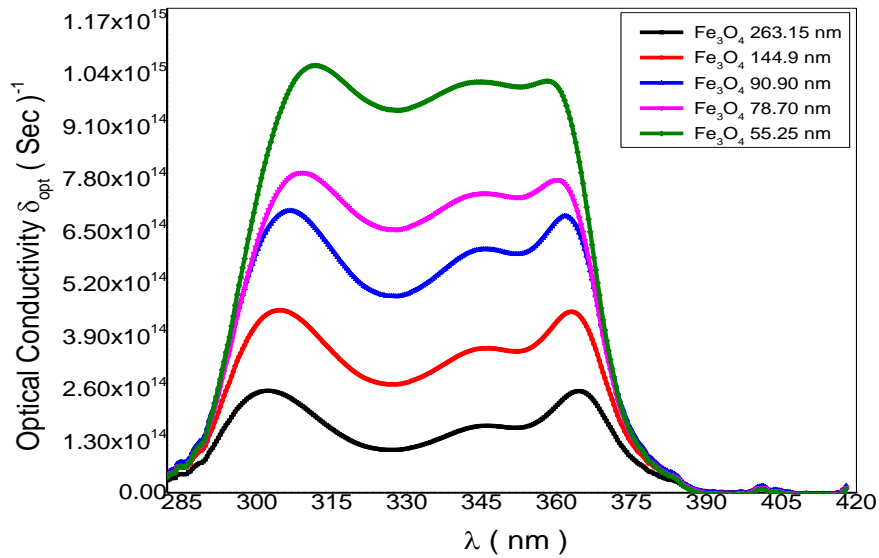
Fig (5.53) The relation between optical conductivity and wavelengths of five sample that made by Fe$_3$O$_4$ in different thickness
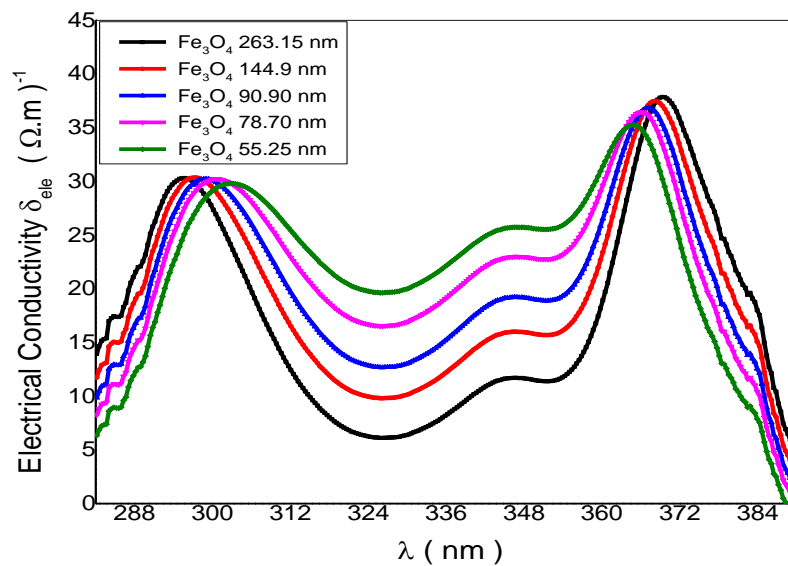
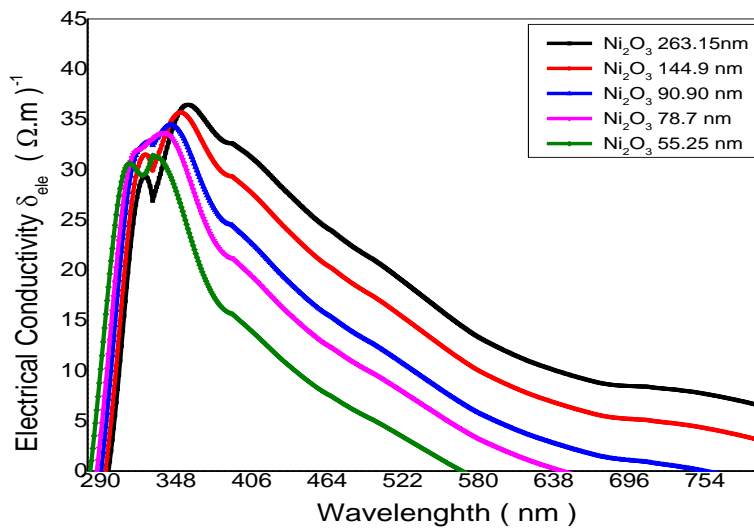**Fig (5.54) The relation between electrical conductivity and wavelengths of five sample that made by Fe$_3$O$_4$ in different thickness**

## 5.3 Discussion

The XRD spectra for Fe_3O_4 and Ni_2O_3 in figures (5.1) and (5.7) are used to determine the Nano crystal size and density for Fe_3O_4 and Ni_2O_3 in tables (5.1) and (5.3) respectively. Table (5.4) beside figures (5.11) and (5.12) shows that the electric permittivity and magnetic permeability of Fe_3O_4 decreases as its concentration increase. But according to table (5.3) the increases too as the concentration increase but the number of Nano crystals n_s which is equal to

$$n_s = \frac{Area}{crystal\ size} = \frac{A}{x_s} \tag{5.1}$$

Decreases, thus μ and ε decreases as the number of Nano crystals decreases. This means that each Nano crystal act as a single electric and magnetic dipole. Thus decrease of n_s decrease both μ and ε according to the relations

$$B = \mu H = \mu_0(H + n_s X_s H) = \mu_0(1 + n_s X_s)H \tag{5.2}$$

$$D = \varepsilon E = \varepsilon_0 E + \varepsilon_0 n_s X_{es} E = \varepsilon_0(1 + n_s X_{es})E \tag{5.3}$$

However the saturation is different for Ni_2O_3, where the increase of its concentration n increases its electric permittivity ε and magnetic permeability μ. This means that the Ni_2O_3 molecules themselves acts as electric and magnetic dipoles according to the relations

$$B = \mu H = \mu_0(H + n_s X_m H) = \mu_0(1 + n_s X_m)H \tag{5.4}$$

$$D = \varepsilon E = \varepsilon_0 E + \varepsilon_0 n_s X_e E = \varepsilon_0(1 + n_s X_e)E \tag{5.5}$$

For Ni_2O_3 table (5.3) shows that increase of N_i concentration increases its crystal size X_s. Thus increase of crystal size increases of the Ni magnetic permeability. Fortunately the results of magnetic permeability for Fe oxides obtained by Amyn S.Teja etal [68] agreas with our resluts, where they show that the permeability for bulk Fe less than the Nano particles and it increases as the Nano size decrease.it is very striking also to find that our resluts for Ni oxide agreas also with the work done by Fardin Taghizadeh [39], where he shows that the magnetic permeability of the bulk Ni oxide is (55Oe) is higher than that of Nano particles (53.8Oe). This means that increase of Nano size increases magnetic permeability.

The absorption spectral pattern, the absorption coefficient and energy gap for Fe_3O_4 and Ni_2O_3 show very interesting properties. For Fe_3O_4, fig (5.44) shows that the absorption peak for all thicknesses is around the wavelength 320 nm. However slight wavelength decrease upon increasing concentration is observed. This means that the absorption peak and pattern are slight dependent on material density and thickness. This means that increasing Fe_3O_4 concentration decrease the absorbed photon wavelength thus increases the minimum photon threshold energy which cause electrons to transfer from valence to conduction band. This means that the increase of Fe_3O_4 concentration increase the energy gap. This agrees with energy gap curve in fig (5.49). According to fig (5.44) the increase of concentrations to take the values (55.25, 78.7, 90.9 144.9 and 263.15) mg/cm^2 causes the wavelength to take values 323, 321, 320, 318 and 317 nm which decreases upon increasing the Fe_3O_4 concentration. The energy gap increases also when the concentration increases and wavelength decrease where it takes the values (3.285, 3.300, 3.308, 3.329 and 3.352) ev respectively. The absorption peaks in the range of 320 nm corresponds to energy gap having order of 3.3 ev. The same hold for Ni_2O_3 where the increase of Ni_2O_3 concentration to take the values (55.25, 78.7, 90.9 144.9 and 263.15) mg/cm^2 causes the wavelengths to decrease to take the values (268, 267, 266, 265 and 264) nm respectively with increase of energy gab to assume the values (3.245, 3.272, 3.283, 3.364 and 3.461) ev respectively. It is very interesting to note that the absorption peaks in the range of 360 nm correspond to energy gabs having order of magnitude in the range of 3.2 ev. Fig (5.47) and fig (5.36) shows that the absorption coefficient increases when the Fe_3O_4 and Ni_2O_3 concentration decrease. This feature can be easily described by using equation (14) which shows inverse relation between the concentrations and absorption coefficient. The fact that the Fe_3O_4 and Ni_2O_3 have large energy gaps in the range ($\sim 3ev$), means that increasing their concentrations n_0 does not increase the concentrations of free carriers n, Thus upon increasing n_0, n remains constant, thus α decrease according to the relation (14)

$$\alpha \sim \frac{n}{n_0} \qquad\qquad (5.6)$$

This may be also explained by suggesting that Fe_3O_4 and Ni_2O_3 are more transparent than the substrate, since they contain a lot of oxygen thus they reemit the absorbed radiation. It is also very interesting to note that the increasing Fe_3O_4 and Ni_2O_3 concentration increases the energy gap. This may be explained by bearing in mind that increasing concentrations decrease the absorption α. But

$$\alpha = (hf)^{-1} C^{\frac{1}{2}} (hf - E_g)^{\frac{1}{2}} \tag{5.7}$$

According to this relation α decrease as the energy gap increases. The increase of energy gap when the Fe_3O_4 and Ni_2O_3 concentrations increase can also be explained by using generalized statistical mechanical laws, by assuming that Nano crystal potential of each Nano particle is an attractive force. Thus the number of particles which is proportional to the concentration is given by:

$$n_0 = A\, e^{\frac{-\beta\, E_g}{\bar{E}}} = A\, e^{\frac{\beta\, E_g}{v}} \tag{5.8}$$

Where: $\quad \bar{E} = -v$

Hence $\quad E_g = \dfrac{v}{\beta} \ln \dfrac{n_0}{A}$

5.4 Conclusions

The electric permittivity and magnetic permeability of Fe_3O_4 are affected by the concentration of Nano crystals where they decrease upon increasing the concentration of Nano crystals. However for Ni_2O_3 the electric permittivity and magnetic permeability are affected by the concentration of the molecules, where they increase upon increasing molecular concentration. The change of Fe_3O_4 and Ni_2O_3 concentrations affects both absorption coefficient and energy gap. The increase of concentration increases the energy gap and decreases the absorption coefficient.

5.5 Recommondation For Future Work

The effect of Nano structure can be also extended to study other ferromagnetic, paramagnetic and diamagnetic substances. The Fe and Ni properties when they are mixed together is also needed. The results obtained can be applied for electric generation and magnetic resonance imaging.

References

[1] M. A. Khan, Mahboob Ullah, Tariq Iqbal, Hasan Mahmood, Ayaz A. Khan, Muhammad Shafique, A. Majid, Azhar Ahmed, and Nawazish A. Khan, (2015) Nanoscience and Nanotechnology Research, Science and Education Publishing, volume (3).

[2] Ali Yadollahpour and Samanehr Ashidi, (2015), Oriental Journal of Chemistry, Volume (31), Pages (25-30).

[3] International Conference on Applied Sciences, IOP Publishing, IOP Conf. Series: Materials Science and Engineering 106 (2016).

[4] A.I.Figueroa, (2015), Magnetic Nanoparticles, Springer Theses, Springer International Publishing Switzerland, Pages (1-12).

[5] H. Shokrollahi L. Avazpour and Particuology, (2016), Volume (26), Pages (32–39).

[6] Hammond, C., (2001) The Basics of Crystallography and Diffraction, 2nd edition, Oxford University Press, New York.

[7] Massa, (2004), Crystal Structure Determination, Springer, New York.

[8] De Graef, M. and M.E.Mc Henry, (2007), Structure of Materials: An Introduction to Crystal graphy, diffraction,and Symmetry, Cambridge University Press, New York.

[9] Eds. R. Advincula and W. Knoll, (2011), Functional Polymer Films, Wiley.

[10] T. Venkatesan, (1996), Thin Solid Films, Volume (52), Pages (216).

[11] Smith,W.F.,and J.Hashemi, (2010), Foundations of Materials Science and Engineering, 5th edition, McGraw-Hill, New York,.

[12] Luisa Filipponi and Duncan Sutherland (2013), Principles, Applications, Implications and Hands-on Activities, Edited by the European Commission, Directorate-General for Research and Innovation Industrial technologies (NMP) programme, pages (19-64).

[13] Cullity B. D., and S. R. Stock, (2001), Elements of X-Ray Diffraction, 3rd edition.

[14] Clarke, A. R., and C. N. Eberhardt, (2002), Microscopy Techniques for Materials Science, CRC Press, Boca Raton, FL,.

[15] Ankur Choudhary, Oct (2017), the principle of Ultra Violet (UV Spectrophotometer).

[16] Fox, M., (2001), Optical Properties of Solids, Oxford University Press, New York.

[17] Gupta,M.C.,and J.Ballato, (2007) The Handbook of Photonics, 2nd edition, CRC Press, Boca Raton, FL.

[18] Rogers, A., (2008), Essentials of Photonics, 2nd edition, CRC Press, Boca Raton, FL.

[19] Craik, D. J., (2000), Magnetism: Principles and Applications, Wiley, New York.

[20] O'Handley, R. C., (2000), Modern Magnetic Materials: Principles and Applications, Wiley, New York.

[21] Spaldin, N. A., (2003), Magnetic Materials: Fundamentals and Device Applications, Cambridge University Press, Cambridge.

[22] Edward M. Purcell, (1985), Electricity and Magnetism, second edition, volume 2, pages 128

[23] Irene, E. A., (2005) Electronic Materials Science, Wiley, Hoboken, NJ.

[24] Braslavsky, S.E., (2007), Glossary of terms used in photochemistry (IUPAC recommendations 2006), Pure and Applied Chemistry, Volume (79), Pages (293–465).

[25] Taghizadeh, F. (2016), the Study of Structural and Magnetic Properties of NiO Nanoparticles. Optics and Photonics Journal, Volume (6), pages (164-169).

[26] Tayebe Razegh1, Vahid Setoodeh, Siamak Pilban Jahromi (2017), Influence of particle size on Magnetic behaviour of nickel oxide nanoparticles, Journal of Optoelectronical Nanostructures, Volume (2), Pages (2).

[27] Ashwani Kumar Singh1, O. N. Srivastava, Kedar Singh (2017), Shape and Size-Dependent Magnetic Properties of Fe_3O_4 Nanoparticles Synthesized Using Piperidine, Nanoscale Research Letters.

[28] Attarad Ali, Hira Zafar, Muhammad Zia, Ihsan ul Haq, Abdul Rehman Phull, Joham Sarfraz Ali, Altaf Hussain (2016), Synthesis, characterization, applications, and challenges of iron oxide nanoparticles, Nanotechnology, Science and Applications, Volume (9), pages (49–67).

[29] Navin K, Kurchania R (2018). The effect of particle size on structural, magnetic and transport properties of $La0.7Sr0.3MnO_3$ nanoparticles. Ceram Int [Internet], Volume (44), pages (5).

[30] BuiTQ, Ton SN-C, Duong AT, Tran HT (2018). Size dependent magnetic responsiveness of magnetite nanoparticles synthesised by co-precipitation and solvothermal methods. J Sci Adv Mater Devices [Internet]. Volume (3), pages (1)

[31] Zhang B, Zhang B, (2018), Magnetic Properties of Nanomaterials, In Physical Fundamentals of Nanomaterials, Elsevier, pages (387–450).

[32] Soler MAG, Paterno LG, (2017), Magnetic Nanomaterials, In Nanostructures Elsevier. Pages (147–86).

[33] SnehaUpadhyay, September (2016), Journal of Alloys and Compounds, Volume (678), Pages (478-485).

[34] GS Kumar, J Akbar, R Govindan, EK Girija (2016), Journal of Science Advanced Materials and Devices, Elsevier.

[35] V. Ratchagar, K. Jagannathan, December (2016), Journal of Alloys and Compounds, Volume (689), Pages (1088-1095).

[36] P.M.Ponnusamya, S.AgilanaN. Muthukumarasamy, T.S.Senthil, G.Rajesh, M.R.Venkatraman, DhayalanVelauthapillai, (2016), Structural, optical and magnetic properties of undoped NiO and Fe-doped NiO nanoparticles synthesized by wet-chemical process, Materials Characterization, Elsevier, Volume (114), Pages (166-171).

[37] Toshitaka Ishizaki, Kenichi Yatsugi and Kunio Akedo, (2016), Effect of Particle Size on the Magnetic Properties of Ni Nanoparticles Synthesized with Trioctylphosphine as the Capping Agent, Nanomaterials, Volume (6), Pages (172).

[38] Attarad Ali, Hira Zafar, Muhammad Zia, Ihsan ul Haq, Abdul Rehman Phull, Joham Sarfraz Ali, Altaf Hussain, (2016), Synthesis, characterization, applications, and challenges of iron oxide nanoparticles, Nanotechnology, Science and Applications, Volume (9), Pages (49–67).

[39] Fardin Taghizadeh, (2016), The Study of Structural and Magnetic Properties of NiO Nanoparticles, Optics and Photonics Journal, Volume (6), Pages (164-169).

[40] Tayebe Razegh, Vahid Setoodeh, Siamak Pilban Jahromi, (2017), Influence of particle size on Magnetic behaviour of nickel oxide nanoparticles, Journal of Optoelectronic Nanostructures, Volume (2), Pages (2).

[41] Mubarak Dirar etal, (2017), The effect of different concentrations of Zno on solar cell performance, International journal of current Trends in Engineering & Research (UCTER), Volume (3).

[42] Khadija Mohamed etal, (2017), the effect of different concentrations of Cuo on Solar cell performance, International journal of Innovative science, Engineering & Technology, Volume (4).

[43] Thawra AbdElradi etal, (2015), the effect of exchanging of Zno and Cno layers on their performance, International journal of Advance Industrial Engineering, Volume (3).

[44] Ehsan Naderi, Mahmoud Naseri, Dariush Souri, April (2018), The effect of SiO_2 and TiO_2 nanoparticle on physical properties of $SrFe_{12}O_{19}$, nanoparticle Current Applied Physics, Volume (18), Pages (469-476).

[45] Xiubin Hou, Zhixin Xue, Yanzhi Xia, Yimin Qin, Kechang Li, March (2019), Effect of SiO_2 nanoparticle on the physical and chemical properties of eco-friendly agar/sodium

alginate Nano composite film, International Journal of Biological Macromolecules, Volume (125), Pages (1289-1298).

[46] S.F.Hasany, N.H.Abdurahman, A.R.Sunarti, R.Jose, November (2012), Magnetic Iron Oxide Nano particles, Journal of Applied Physics, Volume (9), Pages (561-575).

[47] R. O. Yathisha, Y. Arthoba Nayaka, P. Manjunatha, H. T. Purushothama, K. V. Basavarajappa, April (2019), nanoparticle Physical E: Low-dimensional Systems and Nanostructures, Volume (108), Pages (257-268).

[48] Hina Naz, Rai Nauman Ali, Xingqun Zhu, Bin Xiang, June (2018), Effect of Mo and Ti doping concentration on the structural and optical properties of ZnS nanoparticles, Physical E: Low-dimensional Systems and Nanostructures, Volume (100), Pages (1-6).

[49] M. T. Rahman, Md. Asadul Hoque, G. T. Rahman, M. A. Gafur, M. Khalid Hossain, June (2019), Study on the mechanical, electrical and optical properties of metal-oxide nanoparticles dispersed unsaturated polyester resin, Nano composites Results in Physics, Volume (13).

[50] R. O. Yathisha, Y. Arthoba Nayaka, P. Manjunatha, H. T. Purushothama, K. V. Basavarajappa, April (2019), Study on the effect of Zn2+ doping on optical and electrical properties of CuO nanoparticles, Physical E: Low-dimensional Systems and Nanostructures, Volume (108), Pages (257-268).

[51] M. T. Rahman, Md. Asadul Hoque, G. T. Rahman, M. A. Gafur, M. Khalid Hossain, June (2019), Study on the mechanical, electrical and optical properties of metal oxide nanoparticles dispersed unsaturated polyester resin, Nano composites Results in Physics, Volume (13).

[52] Adrian Radoń, Patryk Włodarczyk, Aleksandra Drygała, Dariusz Łukowiec, April (2019), Electrical properties of epoxy Nano composites containing Fe_3O_4 nanoparticles and Fe_3O_4 nanoparticles deposited on the surface of electrochemically exfoliated and oxidized graphite, Applied Surface Science, Volume (474), Pages (66-77).

[53] Zhigang Yang, Zhijia Zhao, Jianbo Yu, Jingyun Li, Gang Yu, June (2019), Effect of Co substitution and magnetic field on the morphologies and magnetic properties of CeO_2 nanoparticles, Ceramics International, Volume (45), Pages (11927-11933).

[54] Hyung Joon Kim, Hyunkyung Choi, August (2019), Effect of plasma treatment on magnetic properties and heating efficiency of Ni-Zn nanoparticles, Journal of Magnetism and Magnetic Materials, Volume (484), Pages (14-20).

[55] I. P. Duru, E. Ozugurlu, L. Arda, April (2019), Size effect on magnetic properties of Zn0.95−xMgxNi0.05O nanoparticles by Monte Carlo simulation, Ceramics International, Volume (45), Pages (5259-5265).

[56] Yi Huang, Xiaomin Cheng, Yuanyuan Li, Dawei Shi, Kai Xu, December (2018), Effect of sol-gel combustion synthesis of nanoparticles on thermal properties of KNO_3-$NaNO_3$,Solar Energy Materials and Solar Cells, Volume (188), Pages (190-20).

[57] Anna Kaźmierczak-Bałata, Jacek Mazur, June (2018), Effect of carbon nanoparticle reinforcement on mechanical and thermal properties of silicon carbide ceramics, Ceramics International, Volume (44), Pages (10273-10280).

[58] Vaibhav Koutu, Oroosa Subohi, Lokesh Shastri, M. M. Malik, September (2018), Study the effect of dip in reaction temperature on thermal and electrical properties of ZnO nanoparticles, Advanced Powder Technology, Volume (29), Pages (2061-2069).

[59] Saebom Ko, Chun Huh, January (2019), Use of nanoparticles for oil production applications, Journal of Petroleum Science and Engineering, Volume (172), Pages (97-114).

[60] Amit Khurana, Sravani Tekula, Mohd Aslam Saifi, Pooladanda Venkatesh, Chandraiah Godugu, March (2019), Therapeutic applications of selenium nanoparticles, Biomedicine & Pharmacotherapy, Volume (111), Pages (802-812).

[61] Surendra Gulla, Dakshayani Lomada, Vadali V. S. S. Srikanth, M. V. Shankar, Madhava C. Reddy, May (2019), Recent advances in nanoparticles-based strategies for cancer therapeutics and antibacterial applications, Methods in Microbiology.

[62] Scriven, L.E., (1988), Physics and applications of dip coating and spin coating.

[63] Emslie, A. G.; Bonner, F. T.; Peck, L. G. (1958), Flow of a viscous liquid on a rotating disk, J. Appl. Phys.

[64] Wilson, S. K., Hunt, R., Duffy, B. R. (2000), the rate of spreading in spins coating, J. Fluid Mech.

[65] Hanaor, D.A.H., Triani, G., Sorrell, C.C. (2011), Morphology and photo catalytic activity of highly oriented mixed phase titanium dioxide thin films, Surface and Coatings Technology.

[66] Niranjan sahu, B parija and S panigrahi, (2009), Fundamental understanding and modelling of spin coating process, Indian J. Physic, Volume (83), Pages (493-502).

[67] Beatriz M. de Campos, Gabriela S. Freiria, Katia J. Ciuffia, Emerson H. de Fariaa, Lucas A. Rochaa, Eduardo J. Nassar, Milton S. F. de Lima, (2017), ITO Obtained by Spray

Pyrolysis and Coating on Glass Substrate, Journal of the Brazilian Chemical Society, volume (28).

[68]Amyn S. Teja, Pei-Yoong Koh, (2009), Synthesis, properties, and applications of magnetic iron oxide nanoparticles, Progress in Crystal Growth and Characterization of Materials, volume (55), pages (22-45).